Review

Electroreduction of CO_2 in Ionic Liquid-Based Electrolytes

Dexin Yang,[1,2] Qinggong Zhu,[2,3,*] and Buxing Han[2,3,*]

Electroreduction of carbon dioxide (CO_2) to value-added chemicals and fuels is a promising approach for sustainable energy conversion and storage. Many electrocatalysts have been designed for this purpose and studied extensively. The role of the electrolyte is particularly interesting and is pivotal for designing electrochemical devices by taking advantage of the synergy between electrolyte and catalyst. Recently, ionic liquids as electrolytes have received much attention due to their high CO_2 adsorption capacity, high selectivity, and low energy consumption. In this review, we present a comprehensive overview of the recent progress in CO_2 electroreduction in ionic liquid-based electrolytes, especially in the performance of different catalysts, the electrolyte effect, as well as mechanism studies to understand the reaction pathway. Perspectives on this interesting area are also discussed for the construction of novel electrochemical systems.

DOI:https://doi.org/10.1016/j.xinn.2020.100016
http://www.cell.com/the-innovation

*Corresponding author:
Email: qgzhu@iccas.ac.cn (Q.Z.), hanbx@iccas.ac.cn (B.H.)

Introduction

Carbon dioxide (CO_2) is a major greenhouse gas. It plays a main role in global warming and leads to serious ecological and environmental problems. It is also a cheap, non-toxic, and abundant C1 feedstock for the production of alcohols, acids, and other value-added chemicals.[1] Recently, many technologies such as thermal, photochemical, and electrochemical methods have been used for CO_2 reduction. However, most thermal catalytic reactions are thermodynamically unfavorable and/or need harsh reaction conditions because CO_2 is thermodynamically stable and kinetically inert.[2] In photocatalytic reactions, the photocatalysts need to absorb light to generate electron-hole pairs with low reaction efficiency.[3] Among the numerous approaches, electrochemical reduction represents a promising approach owing to its high efficiency, simple operation, and mild conditions, providing potential opportunities for large-scale practical applications.[4–11]

Electrochemical reduction of CO_2 is a multi-electron/proton transfer process, which usually includes the following four steps: (1) CO_2 dissolution and adsorption on the catalyst surface, (2) one-electron reduction of CO_2 to $CO_2^{\bullet-}$ free radical, (3) further electron/proton transfer for the generation of the target product, and (4) desorption of the product into the electrolyte or gaseous product escape from the electrolyte. Therefore, the electrochemical reduction products can be controlled via changing reaction parameters such as the electrolyte, electrocatalyst, and applied voltage.[12–15] However, an efficient and selective CO_2 reduction reaction is not trivial because of the chemical inertness of CO_2 molecules, and a large overpotential is often needed to improve the kinetically sluggish

[1]College of Chemistry, Zhengzhou University, Zhengzhou 450001, China;
[2]Beijing National Laboratory for Molecular Sciences, Key Laboratory of Colloid and Interface and Thermodynamics, Institute of Chemistry, Chinese Academy of Sciences, Beijing 100190, China;
[3]University of Chinese Academy of Sciences, Beijing 100049, China

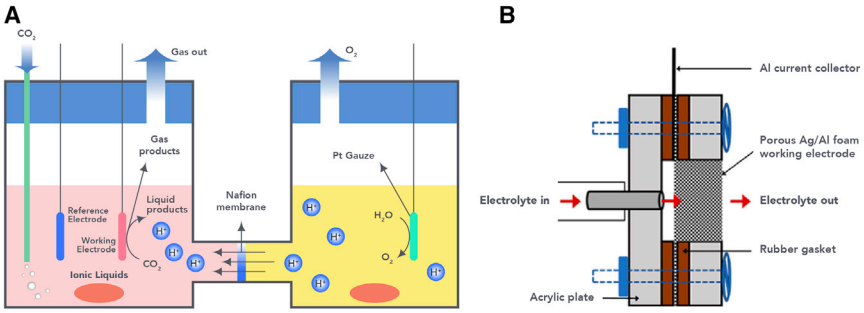

Figure 1 Typical Electrochemical Cells for CO_2 Reduction in IL-Based Electrolytes

(A) H-type and (B) flow cell. Reproduced with permission from Vedharathinam et al.[34] Copyright 2019, ACS Publishers.

reduction process. One resolution is to explore efficient electrochemical systems, including the catalyst and electrolyte, to boost the catalytic performance of CO_2 reduction.[16–27]

Accordingly, the selection of the electrolyte is important in designing efficient electrochemical devices.[28–34] The electrolyte provides a medium for the reduction process, including interactions among the electrode surface, reactants, and intermediates, which in turn influence the reaction pathway.[28] Therefore, the type and composition of the electrolytes play important roles in the reduction reaction. So far, various electrolytes, such as aqueous electrolytes, organic electrolytes, and ionic liquids (ILs) have been applied in CO_2 reduction.[26,28] Among them, ILs have attracted much attention as an electrolyte, and many catalytic reactions have been successfully carried out in this medium for green chemistry.[32]

ILs are composed of cations and anions and have been proven to be a promising new class of environmentally benign solvents.[32] They have also attracted extensive interest owing to their unique properties, such as nearly zero vapor pressure, high electrical conductivity, high electrical and thermal stability, and high gas solubility. In particular, their negligible vapor pressure, high ionic conductivity, and wide electrochemical windows make them excellent alternatives to conventional electrolytes in electrochemical applications.[33] Moreover, ILs also exhibit excellent activity in the electroreduction of CO_2. They provide a medium for CO_2 reduction, and their strong absorption capacity for CO_2 promotes the CO_2 reduction reaction effectively. More importantly, the selectivity of CO_2 reduction can be significantly increased, and the hydrogen evolution reaction (HER) is suppressed in the presence of ILs.[32] In recent years, electrochemical reduction of CO_2 has undergone significant progress in IL-based electrolytes.

In this review, we introduce the current progress of CO_2 electrocatalytic reduction in IL-based electrolytes. Various types of catalysts for producing the target products and the main factors for determining the efficiency are discussed. Moreover, some interesting results associated with the electrolyte effect and mechanism studies in understanding the reaction pathway are also described. Finally, the perspectives in this area are proposed for further study.

Fundamentals of CO_2 Electroreduction in IL-Based Electrolytes

Typical Cell

Typical CO_2 reduction cells in IL-based electrolytes are presented in Figure 1, including H-type cells and flow cells. In an H-type cell (Figure 1A), the cathode and anode are separated by a proton exchange membrane that only allows the transfer of corresponding ions. The membrane takes advantage of independent variation and prevents further oxidation of the products formed from CO_2 reduction. The oxygen evolution reaction and CO_2 reduction occur at the anode and cathode, respectively. In a flow cell (Figure 1B),[34] the electrolyte is in a flow-through configuration to maximize the solubility of CO_2, to overcome mass transport limitations, and to suppress the HER in flow electrolyte.

Table 1. Selected CO_2 Reduction Process in IL-Based Electrolyte and the Corresponding Standard Potentials E^o (pH 7 in Aqueous Solution versus SHE at 25°C, 0.1 MPa, and 1 M Concentration of Other Solutes)

Electrochemical Reduction	E^o (V versus SHE)
CO_2 (g) + e^- ⇌ $CO_2^{\bullet-}$	−1.90
CO_2 (g) + $2H^+$ + $2e^-$ ⇌ HCOOH (l)	−0.61
CO_2 (g) + $2H^+$ + $2e^-$ ⇌ CO (g)+ $2OH^-$	−0.52
CO_2 (g) + $6H^+$ + $6e^-$ ⇌ CH_3OH (l) + H_2O (l)	−0.38
CO_2 (g) + $8H^+$ + $8e^-$ ⇌ CH_4 (g)+ $2H_2O$ (l)	−0.24
$2H^+$ + $2e^-$ ⇌ H_2 (g)	−0.42

Reproduced with permission from Zhang et al.[35] Copyright 2017, Wiley Publishers.

Proposed Pathways for CO_2 Electroreduction

So far, the electroreduction of CO_2 can proceed via two-, six-, and eight-electron reduction pathways in IL-based electrolytes. CO_2 can reduce to species including carbon monoxide (CO), formic acid/formate (HCOOH/$HCOO^-$), methanol (CH_3OH), methane (CH_4), and acetic acid (CH_3COOH). From a thermodynamic perspective, the equilibrium potentials (E^o) of CO_2 reduction and HER are illustrated in Table 1.[35] In CO_2 reduction, the rearrangement of a linear molecule to a bent radical anion ($CO_2^{\bullet-}$) requires enormous energy, which occurs at −1.90 V versus the standard hydrogen electrode (SHE). Therefore, it is difficult to convert CO_2 to the desired product with high efficiency and selectivity by commonly used electrode materials in aqueous electrolytes, although the $CO_2^{\bullet-}$ radical obtained is highly reactive and can form target products after several proton and electron transfer approaches. A more negative potential than E^o is often needed to drive this reaction. In other words, the large overpotential is mainly attributed to the first step of CO_2 electroreduction.

ILs for CO_2 Electroreduction

The structures of typical ILs for electrochemical reduction of CO_2 are depicted in Table 2. In CO_2 reduction, the structure of ILs allows them to coordinate with CO_2, which promotes CO_2 adsorption on the catalyst surface and reduces the energy barrier for CO_2 activation. Hence, the current density and reaction selectivity can be improved. Rosen et al.[36] found that in the presence of 1-ethyl-3-methylimidazolium tetrafluoroborate ([Emim]BF_4), the cell overpotential of CO formation from CO_2 electroreduction could be reduced to 0.17 V on a bulk Ag electrode. To date, many imidazolium-based ILs such as [Emim]BF_4, 1-butyl-3-methylimidazolium tetrafluoroborate ([Bmim]BF_4), and 1-butyl-3-methylimidazolium hexafluorophosphate ([Bmim]PF_6) have exhibited excellent performance in CO_2 electroreduction.[32,37,38] So far, many achievements have been realized in CO_2 electroreduction with IL-based electrolytes. The major merits of IL as an electrolyte and co-catalyst for CO_2 electroreduction not only reflect its strong absorption capacity of CO_2 but also demonstrate that the IL can (1) suppress the competing HER, (2) lower the reduction overpotential, and (3) increase the selectivity for target products.

Catalysts for CO_2 Electroreduction in IL-Based Electrolytes

Various catalysts have been used in CO_2 reduction in IL-based electrolytes, ranging from homogeneous to heterogeneous catalysts. The interactions of CO_2 and/or imidazolium with catalysts play important roles in the efficiency of CO_2 reduction. The electrocatalysts and the applied potentials can significantly affect the current density and the selectivity of the target products. In general, different reduction products, such as CO, HCOOH/$HCOO^-$, CH_3OH, CH_4, and CH_3COOH can be obtained by controlling the reaction conditions of CO_2 electroreduction.

Homogeneous Catalysts

The homogeneous catalysts are generally organic or organometallic compounds, which have intrinsic molecular structures. Therefore, they dissolve in the electrolytes to facilitate the electron and proton transformation during CO_2 reduction. Kubiak et al.[39] summarized the mechanism of homogeneous electrocatalysts used for electroreduction of CO_2 in various electrolytes and elaborated on the electron sources of catalysts (Figure 2). In this case, the reduction of CO_2 and the homogeneous catalyst can occur simultaneously. Therefore, CO_2 reduction usually exhibits favorable kinetics with low overpotentials.

Table 2. Cations and Anions of the Most Commonly Used ILs for CO_2 Electroreduction

Cations			
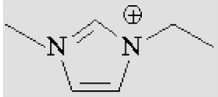	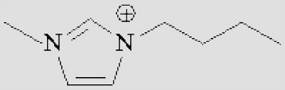	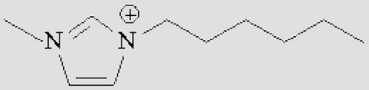	
$[Emim]^+$	$[Bmim]^+$	$[Hmim]^+$	
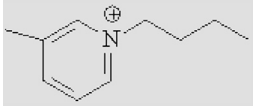	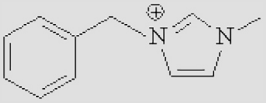	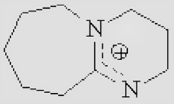	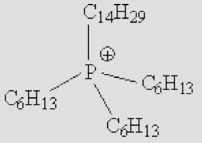
$[Bmpy]^+$	$[Bzmim]^+$	$[DBU\text{-}H]^+$	$[P_{6614}]^+$
Anions			
$[BF_4]^-$	$[PF_6]^-$ X^- (Cl^-, Br^-, I^-)	$[ClO_4]^-$	$[HSO_4]^-$
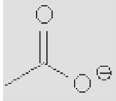	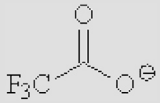	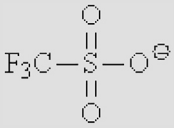	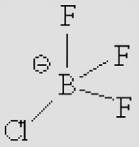
$[Ac]^-$	$[TFA]^-$	$[TFO]^-$	$[BF_3Cl]^-$
$[H_2PO_4]^-$	$[NO_3]^-$		
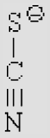	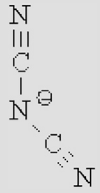		
$[SCN]^-$	$[DCA]^-$		
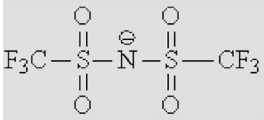	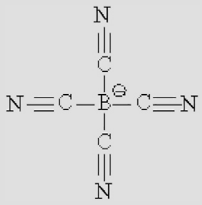	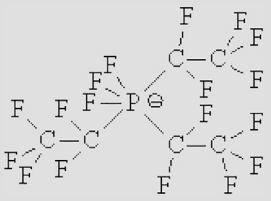	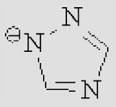
$[NTf_2]^-$	$[TCB]^-$	$[FAP]^-$	$[124Triz]^-$

Owing to the unique properties of IL, homogeneous catalysts have been studied in various IL-based electrolytes. As an example, *fac*-ReCl (2,2′-bipyridine) $(CO)_3$ was initially used as a homogeneous catalyst for electroreduction of CO_2 to CO in 1-ethyl-3-methylimidazolium tetracyanoborate ([Emim]TCB) at a lower overpotential.[40] The rate constant of the apparent CO_2 reduction (k_{app}) in [Emim]TCB was up to 4,000 M^{-1} s^{-1} at 25 ± 3°C. The authors proposed that the interaction between catalysts and $[Emim]^+$ cations accelerated the dissociation of chloride and reduced the activation energy of CO_2 reduction. In another study, the addition of $[Bmim]BF_4$ to the aprotic electrolyte could serve as a proton source and promote *in situ* formation of Fe Porphyrin (FeTPP) conversion to $[Fe^0TPP]^{2-}$ homogeneous catalyst at a less negative potential.[41] Co-catalysis coupling of the IL and homogeneous catalyst for CO_2 reduction exhibited a high faradaic efficiency (FE) of CO (93%) at low overpotential (670 mV) (Figure 3A). Compared with the electrolytes without IL, the turnover number and turnover frequency (TOF) were both increased 4-fold in this system. Isaacs et al.[42] investigated the catalytic activity of $[M^{n+}(cyclam)Cl_n]$ (M = Ni^{2+} and Co^{3+}, cyclam = 1,4,8,11-tetraazacyclotetradecane) homogeneous catalyst in $[Bmim]BF_4$ and 1-butyl-3-methylimidazolium bis(trifluoromethylsulfonyl)imide ([Bmim]NTF_2) electrolytes. Interestingly, they observed that the diffusion coefficient and heterogeneous electron transfer rate of the complexes mainly depended on the anion of IL, which had excellent catalytic performance for CO formation in $[Bmim]BF_4$. In addition, $[Ni(cyclam)Cl_2]$ was proved to be an active catalyst (Figure 3B). When the applied potential was −1.4 V versus Ag/AgCl, only CO could be detected, and the TOF could reach 0.73 h^{-1}. After 4 h electrolysis, the nuclear magnetic resonance (NMR) spectra of the electrolyte showed that the electrolysis reactions did not change the chemical structure of $[Bmim]BF_4$, suggesting that $[Bmim]BF_4$

Review

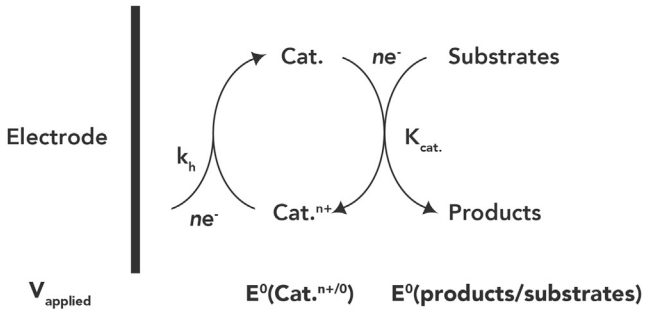

Figure 2 Homogeneous Electrocatalysis with Electron Source

Reproduced with permission from Benson et al.[39] Copyright 2009, RSC Publishers.

was stable during the reaction (Figure 3C). In addition, *in situ* infrared (IR) spectroscopy electrochemical experiments demonstrated that the existence of intermediary Ni(I) from the [Ni(cyclam)Cl_2] catalyst can form a [Ni(cyclam)CO]$^+$ complex and the by-product [$Ni(CO)_4$], which may hinder the generation of CO (Figure 3D).

Heterogeneous Electrocatalysts

In contrast to the above-mentioned homogeneous electrocatalysts, heterogeneous electrocatalysts are low cost and easily recyclable for large-scale applications. The main mechanism of heterogeneous electrocatalysts for electroreduction CO_2 in IL-based electrolytes is shown in Figure 4. In this case, CO_2 reduction mainly occurs at the interface of the electrolytes and heterogeneous electrocatalysts because the electrocatalysts are usually solid and the electrolytes are solvents saturated with CO_2. To date, many catalysts have been exploited, including metal catalysts, metal oxides, metal chalcogenides, and metal-free catalysts.

Metal Catalysts. Metal catalysts, such as Ag, Au, Bi, Cu, etc., have been studied extensively for CO_2 electroreduction in IL-based electrolytes. In the CO_2 reduction reaction, the binding energy between the intermediate and the catalyst surface plays a crucial role in the product distribution.[12,32,35] Generally, some metals (e.g., Sn, Hg, Pb, In) can produce $HCOO^-$ due to their weaker binding energy of $CO_2^{\bullet-}$ intermediate; and some metals (e.g., Au, Ag, Zn, Pd) can bind *COOH tightly, whereas the capability to bind *CO intermediate is weak, and thus CO is the main product with these metals. Among them, Cu has moderate binding energy of *CO intermediate, which provides an opportunity to convert CO_2 to more value-added chemicals with two or more carbon atoms. Cu and Cu-based catalysts as a special category are also be highlighted in this section.

Noble Metal Catalysts. Table 3 provides some results for CO_2 electroreduction on noble metal catalysts in IL-based electrolytes. Rosen et al.[36] reported the use of Ag catalyst for CO_2 reduction in [Emim]BF_4 aqueous solution. They found that IL can act as a homogeneous cocatalyst that improved the catalytic rate, which is ascribed to the extra stabilization of *COOH intermediate. The imidazolium cation can potentially form a complex with CO_2 on the catalyst surface, which may minimize the free energy for the initial electron transfer to CO_2 (Figure 5A). In their following work, they also explored the possible mechanism on a Pt catalyst via sum frequency generation (SFG).[43] The results indicated that a layer of [Emim]$^+$ on the catalyst surface is beneficial to form [CO_2-Emim]$^+$ complex by hindering the HER. By using nonresonant (NR) SFG measurements, they found that little CO was absorbed on the surface of Ag at a threshold potential of −1.33 V versus Ag/AgCl (Figure 5B).[44] When the applied potential shifted negatively, the increase in curvature suggested structural transition of IL driven by the variation of the potential within the double layer (Figure 5C). This suggests that the structural transition of IL and the low overpotential of CO_2 reduction were closely related. Later, Dyson et al.[45] investigated the effect of different imidazolium-based ILs for CO_2 reduction (Figure 5D). In particular, their results showed that the C4 and C5 protons on the imidazolium ring were crucial for enhancing the reaction activity. In another study, trihexyltetradecylphosphonium 1,2,4-triazolide ([P_{66614}]124Triz) was also used as a strongly basic tetraalkyl phosphonium IL to enhance the solubility of CO_2 (Figure 5E).[46] The promotion effect of the IL on CO_2 reduction was also explored. In the reaction, CO_2 could bind to a 1,2,4-triazole anion and was then reduced to $HCOO^-$ at a low overpotential (0.17 V).

Review

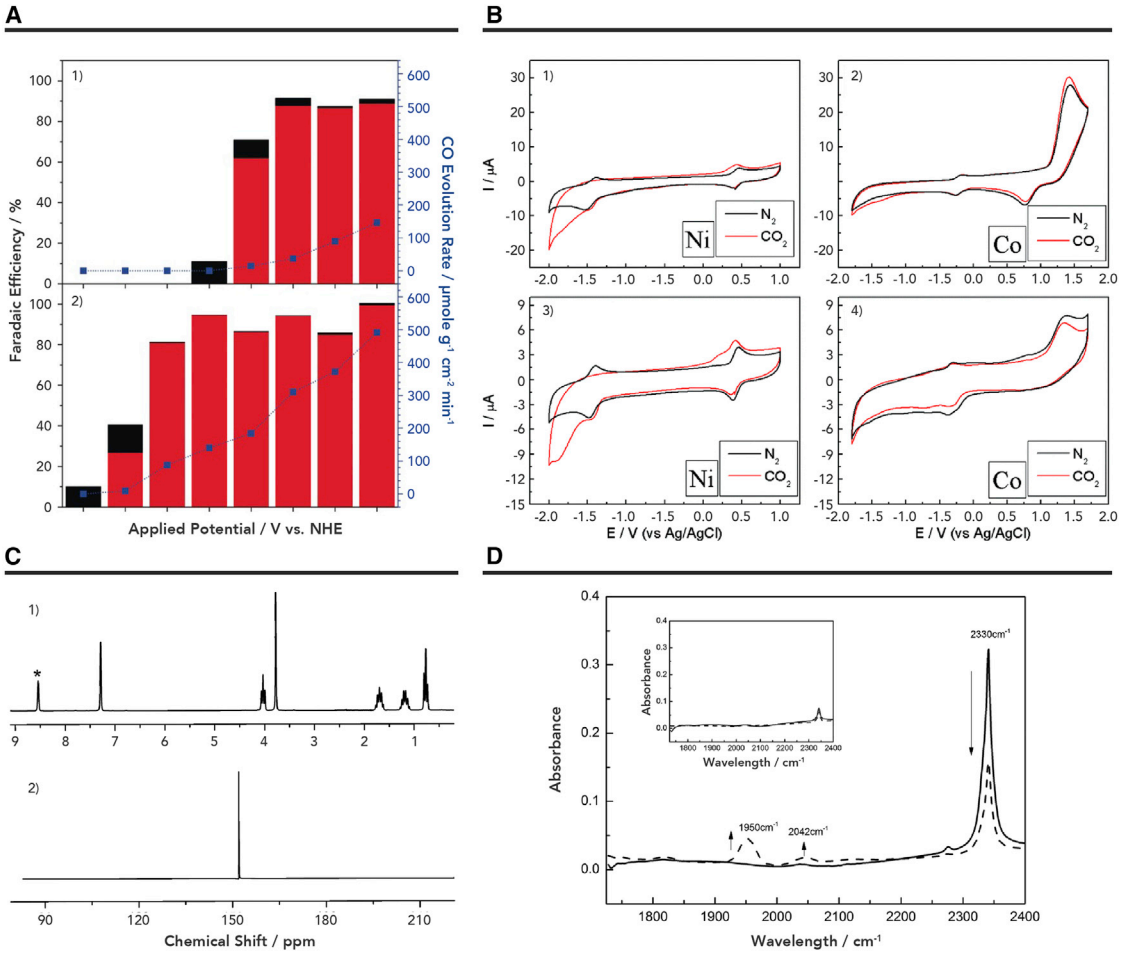

Figure 3 The Performances of Different Homogeneous Catalysts in Various IL-Based Electrolytes

(A) FEs for CO (red bar)/H_2 (black bar) and CO (blue line) evolution rates at various applied potentials under a CO_2 atmosphere. (1) 0.5 mM Fe^{III} PPCl +1 M TFE; (2) 0.5 mM Fe^{III} TPPCl +1 M TFE + 0.3 M [Bmim]BF_4. Reproduced with permission from Choi et al.[41] Copyright 2014, Wiley Publishers.

(B) Electrochemical behavior of the system in [Bmim]BF_4 (1 and 2), and in [Bmim]NTF_2 (3 and 4), [Ni(cyclam)Cl_2] and [Co(cyclam)Cl_2]Cl at 9.7 mM and 2 mM respectively, both saturated with N_2 (black line) and CO_2 (red line), at 100 mV/s.

(C) H^1-NMR (1) and (2) F^{19}NMR spectra of [Bmim]BF_4 after 4 h of potential-controlled electrolysis at −1.4 V versus Ag/AgCl.

(D) Infrared *in situ* spectroelectrochemical behavior of the [Ni(cyclam)Cl_2] complex in [Bmim]BF_4 saturated with N_2 (insert) and CO_2 at open circuit potential (solid line) and after 10 min of electrolysis at −1.4 V (dashed line). Reproduced with permission from Honores et al.[42] Copyright 2017, RSC Publishers.

Au has also attracted wide attention because of the excellent performance of CO_2 conversion in IL-based electrolytes. An early report from Zhu et al.[47] explored the catalytic activity of CO_2 reduction over Au nanoparticles in [Bmim]PF_6-based electrolyte. In the presence of IL, the intermediate COOH* could be stabilized efficiently on the Au catalyst. In a later study, electrochemical impedance spectroscopy was applied to determine the difference in interface character between 1-butyl-3-methylimidazolium trifluoromethanesulfonate ([Bmim]CF_3SO_3)/propylene carbonate (PC) and tetrabutylammonium trifluoromethanesulfonate ([Bu_4N]CF_3SO_3)/PC over Au catalyst.[48] The authors considered that [Bmim]$^+$ would be absorbed on the surface of the catalyst, resulting in the generation of IL film. During the reaction, the formation of [Bmim-CO_2]$_{(ad)}$ could be a benefit for decreasing the activation energy and overpotential of CO_2 electroreduction. Cuesta et al.[49] combined *in situ* surface-enhanced infrared absorption spectroscopy in attenuated total reflection mode (ATR-SEIRAS) with cyclic

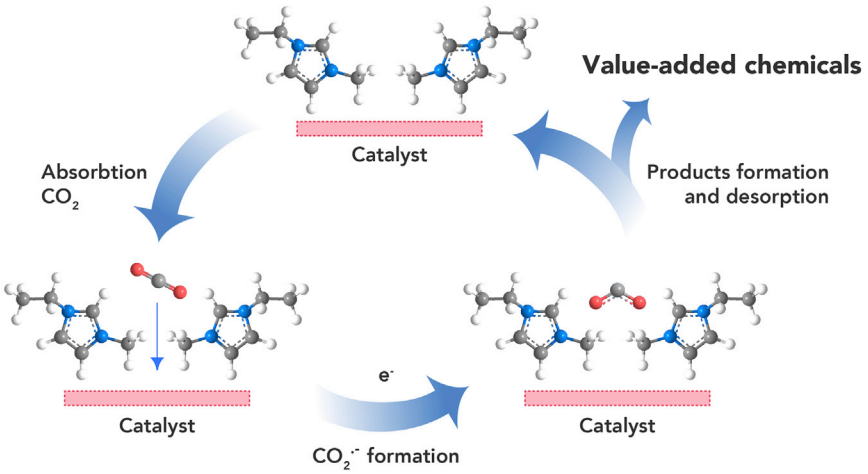

Figure 4 The Main Mechanism of Heterogeneous Electrocatalysts for Electroreduction CO_2 in IL-Based Electrolytes

voltammetry (CV) to study the reason for the decreasing reduction potential of CO_2 in IL (Figure 6A). They attributed this to the lower coverage of the adsorbed layer formed upon CO_2 reduction, which led to a lower degree of dipole-dipole coupling. Then, the CO bands started decreasing at more positive potentials due to CO desorption from the surface. The catalytic ability of CO_2 was also studied on low-index Au(hkl) single crystal catalysts in eight ILs.[50] The Au(110) catalyst exhibited higher activity than Au(111) and Au(100) catalysts. The authors observed that the deactivation of Au(110) catalyst mainly originated from surface reconstruction by *in situ* scanning tunneling microscopy (STM) (Figure 6B).

Pt is another active catalyst for CO_2 reduction. As an example, Compton et al.[51] found electrochemical conversion of CO_2 to HCOOH can occur over anodized Pt wire in 1-ethyl-3-methylimidazolium bis(trifluoromethylsulfonyl)imide ([Emim]NTF_2). The performance of ILs with cyano (–CN) or methoxy ($–OCH_3$) functionalized imidazolium cations was also evaluated as electrolytes for electrochemical reduction of CO_2 on Pt catalyst.[52] The results indicated that the addition of the functional groups in ILs can reduce the activated energy for the formation of $CO_2^{\cdot-}$ intermediate. Consistently, the Pt(110) single crystal catalyst also efficiently promoted electrochemical synthesis of HCOOH from CO_2 in [Emim]NTF_2 electrolyte.[53]

Post-transition Metal Catalysts. Some examples of CO_2 electroreduction on post-transition metal catalysts in IL-based electrolytes are given in Table 3. Typically, Bi is an abundant, inexpensive, and non-toxic post-transition metal. It is widely probed in electrochemical conversion CO_2 to CO or $HCOO^-$ with IL-based electrolytes. Rosenthal et al.[64] reported pioneering work that utilized Bi film as the cathode for CO_2 reduction in acetonitrile containing $TBAPF_6$ and [Bmim]PF_6 as supporting electrolyte. In this system, the FE of CO could reach approximately 95% at a very low overpotential. In their following work, they also found ILs containing different cations as electrolytes affected the selectivity for CO_2 reduction over Bi cathodes (Figure 6C).[66] Recently, Zhu et al.[67] designed surface-activated Bi nanoparticles (NPs) for electrochemical reduction of CO_2 to CO in [Bmim]OTF/acetonitrile electrolyte. The FE of CO can reach 96.1%, and the mass activity for CO evolution (MA_{CO}) can achieve 15.6 mA mg^{-1} over activated 36-nm Bi NPs (Figure 6D). Furthermore, the structure of Bi was studied during cathodic polarization in acetonitrile solution containing $[Bmim]^+$-based ILs.[75] The authors observed that the Bi_2O_3 layer on the Bi (001) films was reduced during the first CV scan, and Bi could gradually dissolve in lateral size in the CV scans between −1.5 V to −1.9 V versus Ag/AgCl (Figure 6E). The authors also found that the generation of a Bi···$[Im]^+$ complex was beneficial for CO_2 reduction.

CO_2 electroreduction on other post-transition metals, such as In, Sn, Pb, have also been studied. Rosenthal et al.[69] investigated the catalytic activity of Sn, Pb, Bi, and Sb, which were fabricated by the electrodeposition method. In their study, the electrochemical reduction

Table 3. Selected Examples of CO_2 Electroreduction on Metal Catalysts in IL-Based Electrolytes

Catalysts	Electrolytes	Potential	Current Density (mA cm^{-2})	Main Products	FE for Main Products (%)	References
Noble Metal Catalysts						
Ag	18 mol % [Emim]BF_4/H_2O	1.5 V[a]	–	CO	96	Rosen et al.[36]
Ag	75 μM H_2O/[Emim]BF_4	3.25 V[a]	~4	CO	–	Salehi-Khojin et al.[54]
Ag	0.1 mol L^{-1} [P_{66614}] 124Triz/acetonitrile	−0.7 V versus Ag/$AgNO_3$	–	HCOOH (little amount HCHO)	63	Hollingsworth et al.[46]
Ag	0.02 M 1,3-dimethyl-2-phenyl-imidazolium tetrafluoroborate/0.1 M $TBAPF_6$[b]/7 mL acetonitrile	~ −1.4 V versus Fc^+/Fc[c]	4.2	CO	~100	Lau et al.[45]
Ag	50 mol % [Emim]TFO[d]/ 10 × 10^{-3} M $KHCO_3$/H_2O	−1.80 V versus Ag/AgCl	~10	CO	95.6 ± 6.8	Neubauer et al.[55]
Ag	0.1 M n-Bu_4NPF_6[e]/ 2.0 mM [C_{10}mim]BF_4[f] + 1.0% H_2O/acetonitrile	−2.3V versus Fc^+/Fc[c]	–	H_2	1.8	Zhao et al.[56]
				CO	70.4	
				$C_2O_4^{2-}$	27.1	
				$HCOO^-$	0.4	
Ag	[Bmim]BF_4/H_2O (≤70%)	–	−1	CO	>90	Rudnev et al.[57]
Ag	[Bmim]BF_4/20% H_2O	−1.6 V versus Ag/AgCl	–	CO	>94	Rudnev et al.[58]
Ag	1 M [EmimOH]Cl[g]/2 M EG/PC[h]	−1.7 V versus Ag/AgCl	~4	CO	~100	Vasilyev et al.[59]
Rough Ag	8 mM [POHmim]BF_4[i]/ acetonitrile	−2.5 versus Fc^+/Fc[c]	16.4	CO	92	Zhang et al.[60]
Ag nanoflowers (flow cell with electrolyte flow-through rates of 100 mL min^{-1})	[Emim]BF_4/H_2O (92/8 v/v %)	−1.8 V versus Pt	36.6 (j_{CO}[j])	CO	75	Vedharathinam et al.[34]
Ag, Au, or Pt	0.1 mol L^{-1} [P_{66614}] 124Triz/acetonitrile/ 0.7 mol L^{-1} H_2O	−0.7 V versus Ag/$AgNO_3$	–	$HCOO^-$ (on Ag catalysts) Syngas (on Ag, Au, and Pt)	95 ($HCOO^-$ on Ag catalysts)	Hollingsworth et al.[61]
Au(110)	[Bmim]BF_4	−1.82 V versus Ag/AgCl	~1	CO	95	Fu et al.[50]
Au	0.1 M [Bmim]BF_4/ acetonitrile	−1.73 to −1.93 V versus NHE[k]	–	CO	95	Koh et al.[62]
Au	0.1 mol dm^{-3} [Bmim] OAc[l]/dimethyl sulfoxide/0.2 vol % H_2O	−1.80 V versus Ag/AgCl	8.6	CO	98	Gonçalves et al.[63]
Pt	50 mM H[NTF_2][m]/ [Emim]NTF_2	–	–	$HCOO^-$	–	Martindale et al.[51]
Post-transition Metal Catalysts						
Bi	20 mM [Emim]BF_4/ acetonitrile/0.1 M $TBAPF_6$	−1.95 V versus SCE[n]	5.51 ± 1.2	CO	95 ± 6	DiMeglio et al.[64]
Bi	300 mM [Bmim]OTF[o]/ acetonitrile	−2.0 V versus SCE[n]	25 ± 2	CO	87 ± 8	Medina-Ramos et al.[65]
Bi	250 mM [Bmim]PF_6/ acetonitrile/0.1 M $TBAPF_6$	−1.95 V versus SCE[n]	15 ± 2	CO	84 ± 3	Atifi et al.[66]
				$HCOO^-$	10 ± 2	
	250 mM [DBU-H]PF_6[p]/ acetonitrile/0.1 M $TBAPF_6$		27 ± 3	$HCOO^-$	77 ± 5	
				CO	21 ± 1	
Activated 36-nm BiNPs	100 mM [Bmim]OTF/ acetonitrile	−2.0 V versus Ag/AgCl	15.6 mA mg^{-1}	CO	96.1	Zhang et al.[67]
Sn power	0.5 M [Emim]$N(CN)_2$[q]/H_2O	−1.2 V versus RHE[r]	~0.3 mA	$HCOO^-$	81.9	Zhang et al.[68]
Bi	100 mM [Bmim]OTF/ acetonitrile	−1.95 V versus SCE[n]	10.1 ± 2.1	CO	78 ± 5	Medina-Ramos et al.[69]
Sn		−1.95 V versus SCE[n]	7.2 ± 1.9		77 ± 5	
Pb		−2.05 V versus SCE[n]	5.0 ± 1.0		81 ± 5	

(Continued on next page)

Table 3. *Continued*

Catalysts	Electrolytes	Potential	Current Density (mA cm^{-2})	Main Products	FE for Main Products (%)	References
Sn	30 wt % [Bmim]PF_6/ acetonitrile/5wt %H_2O	−2.3 V versus Ag/Ag^+	32.1 (j_{HCOO^-}[s])	$HCOO^-$	92	Zhu et al.[70]
Pb			37.6 (j_{HCOO^-}[s])		91.6	
Pb	0.1 M [Emim]TNF_2/ 0.1 M TEAP[t]/acetonitrile	−2.34V versus $Ag/AgNO_3$	–	CO carboxylate	–	Sun et al.[71]
Pb	700 mM [Bmim] 124Triz[u]/acetonitrile/ 5 wt % H_2O	−2.4V versus Ag/Ag^+	24.5	$HCOO^-$	95.2	Feng et al.[72]
Pb phytate	12.8 wt % [Bzmim]BF_4[v]/ 9.9 wt % H_2O/acetonitrile	−2.25 V versus Ag/Ag+	30.5	$HCOO^-$	92.7	Wu et al.[73]
In	Dimcarb[w]	−1.34 V versus $Cc^{+/o}$[x]	–	CO	45	Chen et al.[74]
				$HCOO^-$	40	
In	[Bmim]PF_6/acetonitrile/ 1 mM $In(acac)_3$[y]	−1.9 V versus SCE[n]	~15	CO	99	Ding et al.[14]

[a]Cell voltage.
[b]Tetrabutylammonium hexafluorophosphate.
[c]Ferrocene/ferrocenium.
[d]1-Ethyl-3-methylimidazolium trifluoromethanesulfonate.
[e]Tetrabutylammonium hexafluorophosphate.
[f]1-Decyl-3-methylimidazolium tetrafluoroborate.
[g]1-Ethyl-3-methylimidazoliumhydroxide chloride.
[h]Propylene carbonate.
[i]1-(3-Hydroxypropyl)-3-methylimidazolium tetrafluoroboride.
[j]CO partial current density.
[k]Normal hydrogen electrode.
[l]1-Butyl-2,3-dimethylimidazolium acetate.
[m]bis(Trifluoromethane)-sulfonimide.
[n]Saturated calomel electrode.
[o]1-Butyl-3-methylimidazolium trifluoromethanesulfonate.
[p][DBU] is 1,8-diazabicyclo[5.4.0]undec-7-ene.
[q]1-Ethyl-3-methylimidazolium dicyanamide.
[r]Reversible hydrogen electrode.
[s]$HCOO^-$ partial current density.
[t]Tetraethylammonium perchlorate.
[u]1-Butyl-3-methylimidazolium 1,2,4-triazolide.
[v]1-Benzyl-3-methylimidazolium tetrafluoroborate.
[w]Dimethylammonium dimethylcarbamate.
[x]Cc^+ is cobaltocenium.
[y]Indium acetylacetonate.

of CO_2 was performed in acetonitrile/[Bmim]OTF electrolyte. Sn and Bi can efficiently catalyze CO_2 to CO with current densities of 5–8 mA cm^{-2}. In contrast, Pb and Sb cannot favor CO formation. They demonstrated that the IL can enhance the generation of CO by combining with an appropriate catalyst. In addition, Li et al.[14] also found that *in situ* prepared In nanocrystals can efficiently catalyze CO_2 conversion to CO in IL-based electrolytes. Ha et al.[68] reported on [Emim]$N(CN)_2$ aqueous solution as the electrolyte to improve the solubility of CO_2 and inhibit the HER for efficient electroreduction of CO_2 to HCOOH over Sn powder catalyst. The maximum FE of HCOOH can reach 81.9% at −1.2 V versus RHE. In addition, acetonitrile and [Emim]TNF_2 solutions were used as the electrolyte for CO formation from CO_2 electroreduction using Pb as a catalyst.[71] The authors also found that the ratio of acetonitrile and [Emim]TNF_2 changed the pathway of the reaction, reducing the formation of oxalate anion and enhancing CO generation. In addition, electroreduction of CO_2 over Pb or Sn cathodes was reported in ternary mixture electrolytes ([Bmim]PF_6 [30 wt %]/acetonitrile-H_2O) with a partial current density of 37.6 mA cm^{-2} and FE of 91.6% for $HCOO^-$.[70] Interestingly, the authors found that the existence of a small amount of H_2O can significantly enhance the efficiency of the reaction. In another example, In, Sn, and Pb catalysts were also applied in the electroreduction of CO_2 to $HCOO^-$ in

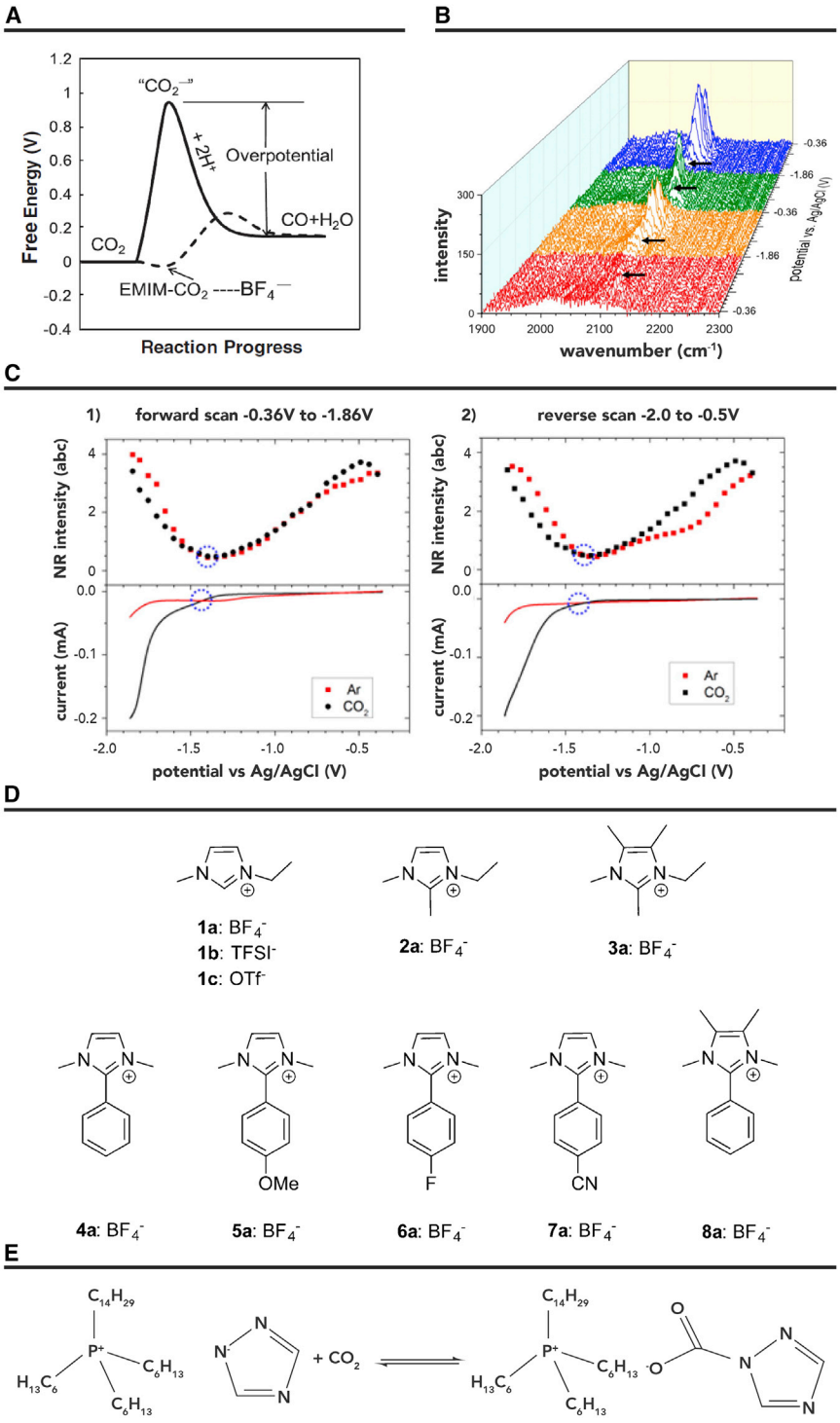

Figure 5 The Results of Different ILs Used as Electrolytes over Ag Catalysts for Electroreduction of CO_2

(A) A schematic illustration of how the free energy of the system changes during the reaction $CO_2 + 2H^+ + 2e^- \rightleftharpoons CO + H_2O$ in H_2O or acetonitrile (solid line) or [Emim]BF_4 (dashed line). Reproduced with permission from Rosen et al.[36] Copyright 2011, AAAS Publishers.

(B) SFG spectra of CO adsorbed on Ag as the potential was scanned from −0.36 to −1.86 V for two cycles. Each major division along the potential axis is equal to 0.5 V. The arrows indicate the threshold potential for CO_2 reduction, −1.33 V.

(C) (Top) SFG nonresonant (NR) signals when IL electrolyte was saturated with Ar or CO_2. (Bottom) Meniscus cyclic voltammetry (CV). The circles denote the threshold potential for CO_2 reduction and the NR intensity minimum. There was a close association between the onset of CO_2 reduction and the nonresonant intensity minimum. (1) First forward (reduction) scan. (2) First reverse (oxidation) scan. Reproduced with permission from García Rey et al.[44] Copyright 2015, ACS Publishers.

(D) Structures of imidazolium salts studied. Reproduced with permission from Lau et al.[45] Copyright 2015, ACS Publishers.

(E) Addition of CO_2 to $[P_{66614}]$124Triz, showing binding of CO_2 to the triazolide anion. Reproduced with permission from Hollingsworth et al.[46] Copyright 2015, Wiley Publishers.

1-ethyl-3-methylimidazolium trifluoroacetate ([Emim]TFA) aqueous solution.[76] The excellent performance was attributed to the high CO_2 solubility in IL and the capacity of IL to stabilize the reaction intermediate.

Cu-Based Catalysts. Different hydrocarbons and alcohols have been obtained from direct conversion of CO_2 on Cu-based catalysts.[35] Dendritic Cu nanomaterials were prepared for CO_2 electroreduction to HCOOH in IL-based electrolyte.[77,78] It was discovered that the synergetic interaction between IL and the structure of the catalyst favors the generation of $HCOO^-$. Bimetallic nanomaterials have also been investigated to improve the catalytic performance by altering the degree of stabilization of key intermediates. On bimetallic Zn-Cu film,

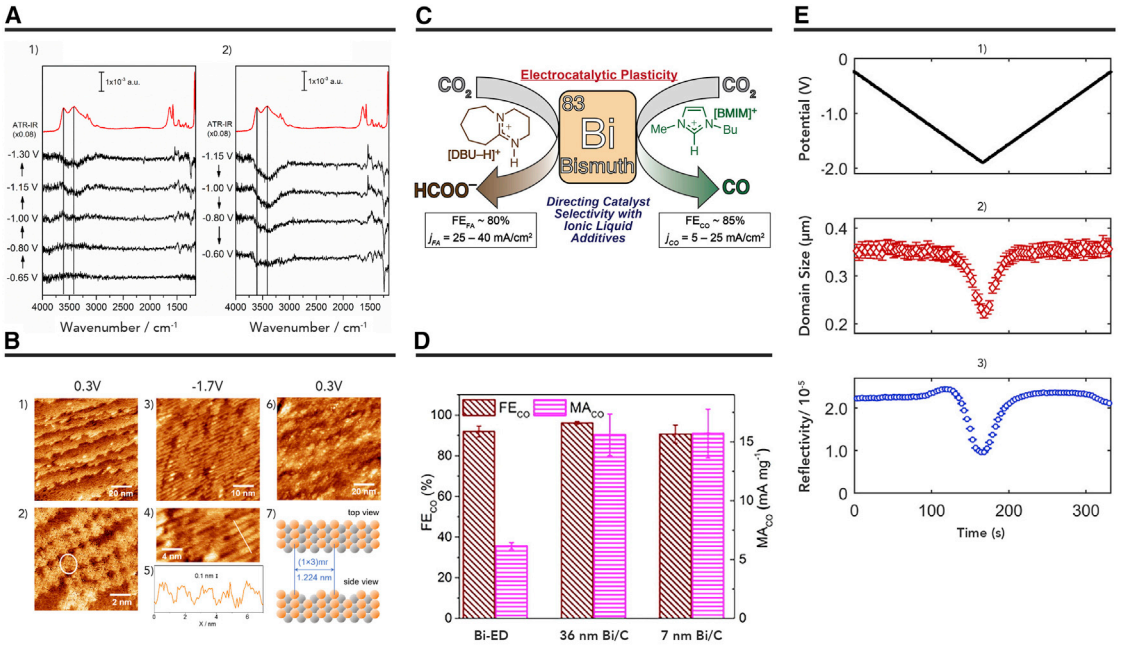

Figure 6 The Preformances of Different ILs for Electroreduction of CO_2

(A) ATR-SEIRA spectra of an Au catalyst in CO_2-saturated [Emim]BF_4/H_2O (18% mol/mol) acquired during the negative-going (1) and positive-going (2) sweeps of a cyclic voltammogram at 5×10^{-4} V s^{-1}. The reference spectrum was taken at −0.60 V just before starting the potential sweep in the negative direction. The highlighted bands correspond to νasym (CO_2), magenta star; ν(COL), blue star; and ν(COB), green star. The red lines correspond to the ATR infrared spectrum of the [Emim]BF_4/H_2O mixture (18% mol/mol) and are included for the sake of comparison. Reproduced with permission from Papasizza et al.[49] Copyright 2018, ACS Publishers.

(B) *In situ* STM images of Au(110) in CO_2-saturated [Bmim]BF_4 (1 and 2) at 0.3 V at the beginning of the experiment, (3 and 4) at −1.7 V and 0.3 V after 1 h exposure of the catalyst at −1.7 V. (5) Cross-sectional profile along the white line in panel (6). (7) Scheme of the missing row reconstruction of Au(110), where every third row is missing. Reproduced with permission from Fu et al.[50] Copyright 2018, Wiley Publishers.

(C) Adjusting the production of CO_2 reduction over bicathodes using varied ILs as electrolytes. Reproduced with permission from Atifi et al.[66] Copyright 2018, ACS Publishers.

(D) FE_{CO} and MA_{CO} on electrodeposited Bi films (Bi-ED), 36-nm and 7-nm freshly reduced Bi/C. Reproduced with permission from Zhang et al.[67] Copyright 2016, ACS Publishers.

(E) Change in lateral size of Bi (001) domains and reflectivity as a function of the applied potential for bismuth thin film cathodes in CO_2-saturated acetonitrile containing 100 mM [Bmim]OTF (1–3). (1) The potential function applied during voltammetry; (2) the Bi (001) lateral domain size change (open red diamonds); (3) the total reflectivity (open blue circles) as a function of time. Reproduced with permission from Medina-Ramos et al.[75] Copyright 2018, ACS Publishers.

the rate of syngas generation can reach 85 N μL (normal microliter) cm^{-2} C^{-1}/170 N μL cm^{-2} h^{-1}.[79] In a recent study, Pd-Cu bimetallic aerogel was used as a catalyst for electrochemical conversion of CO_2 to CH_3OH in electrolytes composed of 25 mol % [Bmim]BF_4 and 75 mol % H_2O.[80] The excellent performance of Pd-Cu aerogels can be attributed to the high porosity of aerogel and the special valence states of the two metals (Figures 7A–7D). The IL-based electrolyte can also adsorb and stabilize $CO_2^{\bullet-}$, which is favorable for CO_2 reduction. CuSn alloys can also efficiently reduce CO_2 in an IL-based electrolyte at low overpotential[81] due to the synergistic effect between two metals.

In addition, Cu-doped catalysts have been explored in the reaction to enhance energy efficiency. For this purpose, Roy et al.[82] investigated CO_2 electroreduction to CO on Cu-modified boron-doped diamond (BDD) in

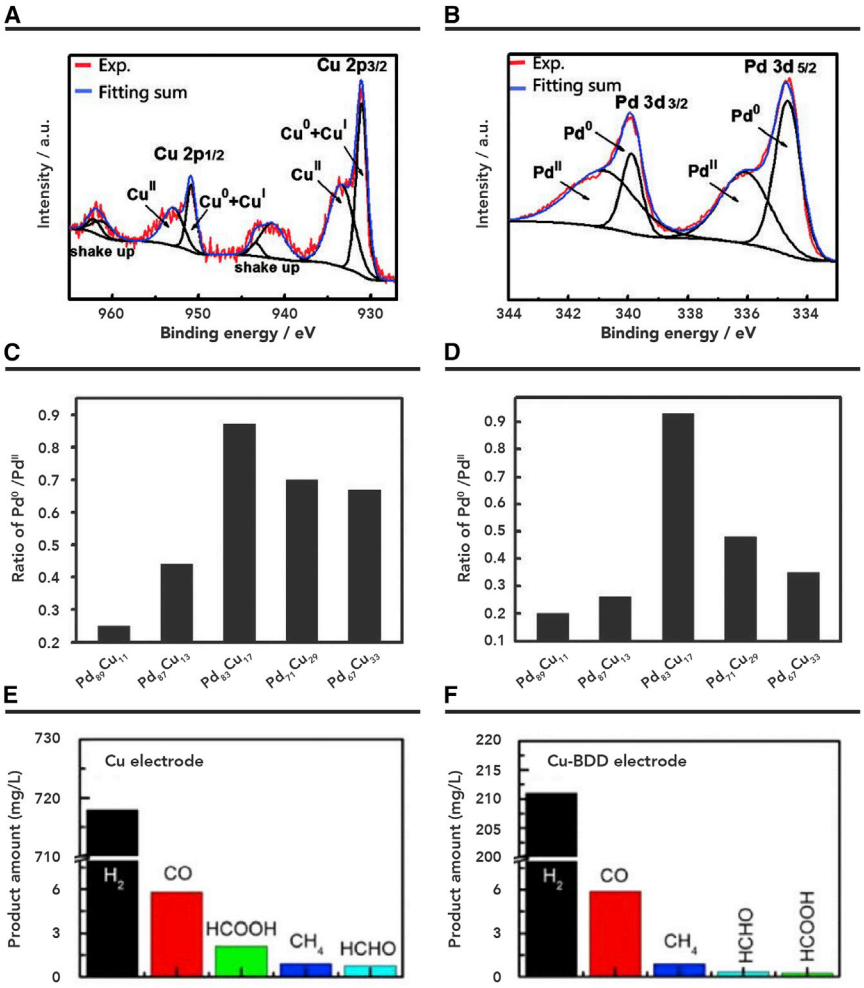

Figure 7 The Results of Different Cu-Based Catalysts with Various IL-Based Electrolytes

(A and B) X-ray photoelectron spectroscopy of (A) Cu 2p and (B) Pd 3d levels of catalysts. (C and D) The relative intensity ratios of (C) Pd^0/Pd^{II} and (D) $Cu^I + Cu^0/Cu^{II}$ in catalysts. Reproduced with permission from Lu et al.[80] Copyright 2018, Wiley Publishers. (E and F) Various gaseous and liquid electrochemical reduction products obtained by using (E) the Cu catalyst and (F) the Cu-modified BDD catalyst in the presence of 100 mM $[Emim]BF_4$ IL at −1.2 V versus SHE. Reproduced with permission from Roy et al.[82] Copyright 2016, Wiley Publishers.

100 mM $[Emim]BF_4$ aqueous solution. Compared with bare Cu, the Cu-modified BDD catalysts can inhibit the HER and enhance product selectivity (Figures 7E and 7F). N-based Cu(I)/C-doped boron nitride (BN-C) composites were also designed for electroreduction of CO_2 in $[Emim]BF_4$-LiI-H_2O electrolyte.[83] The authors found that the current density could reach 13.9 mA cm^{-2} with a high FE for acetic acid of 80.3%. The synergistic effect of Cu complex, substrate, and electrolyte favor the production of the desired product.

Other Transition Metal-Based Catalysts. Besides Cu, other transition metal (Mo, Co, Zn)-based catalysts have been tested in IL-based electrolytes. Xie et al.[84] carried out electroreduction of CO_2 on single Mo atoms loaded on N-doped graphene in 4 mol % $[Emim]BF_4$ aqueous solution, which can favor production of $HCOO^-$. Zhang et al.[85] reported that the electrochemical reduction of CO_2 can be performed on a Cd catalyst derived from $Cd(OH)_2$ in $[Bmim]PF_6$/acetonitrile electrolyte. The FE for CO can reach 99.2% with a partial current density of 59.0 mA cm^{-2}. A Zn metal-organic framework (Zn-MOF) was also used as the cathode in $[Bmim]BF_4$ electrolyte for CO_2 reduction.[86] The FE of CH_4 could reach 80% at a low overpotential of 0.14 V. Furthermore, electroreduction of CO_2 was studied over an indium tin oxide modified by cobalt 5,10,15,20 tetrakis(4-aminophenyl)porphyrin (Co-TAPP) in $[Bmim]BF_4$.[87] The results indicated that Co(I) porphyrin species, which promoted the reaction, were detected in an inert atmosphere rather than in the CO_2-saturated medium.

Metal Oxides and Metal Chalcogenides. So far, some attention have been given to CO_2 reduction on metal oxides and metal chalcogenides, such as MoO_2, SnO_2, and MoS_2. Chu et al.[88] synthesized low-density polyethylene from CO_2 electrochemical reduction over

a nanostructured TiO_2 catalyst in [Emim]BF_4 aqueous solution. The current efficiency of low-density polyethylene was about 8%–14% at an applied potential of −1.50 V versus standard calomel electrode (SCE). Electroreduction of CO_2 was carried out over MoO_2 with [Bmim]PF_6/acetonitrile as electrolyte.[89] The addition of IL in the electrolytes led to lower overpotential and improved the FE of CO. The electrocatalytic performance of commercial PbO_2 was carried out in various catholytes composed of IL, H_2O, and acetonitrile.[90] The [Bzmim]BF_4 was considered to be the best IL for improving the FE of HCOOH. SnO_2 nanosheets on N-doped porous carbon (SnO_2@N-PC) were prepared for CO_2 electroreduction to HCOOH in 0.5 M [Bmim]PF_6 acetonitrile solution.[91] The current density was 28.4 mA cm^{-2} with HCOOH FE of 94.1% at an overpotential of 0.31 V.

Metal chalcogenides can exist in many forms of stoichiometries and structures, therefore they have been widely studied in many fields including CO_2 electrolysis.[35,92–94] For example, titanium disulfide (TiS_2) planes were synthesized for CO_2 electroreduction to CO in IL-H_2O-acetonitrile.[95] The results revealed that cathodic energy efficiencies can be as high as 64% with a current density of 5 mA cm^{-2}. Asadi et al.[96] prepared molybdenum disulfide (MoS_2) for CO_2 electrochemical reduction. The high current density and low overpotential were obtained in 96 mol % H_2O and 4 mol % [Emim]BF_4 solution. In the same electrolyte, N-doped MoS_2 nanosheets and N-doped carbon nanodots (N-MoS_2@NCDs) composite electrocatalyst were synthesized for CO_2 reduction to CO.[97] The good electrical conductivity provided by NCDs on the MoS_2 surface can enhance electron transport. A series of Mo-Bi bimetallic chalcogenides (BMCs) were fabricated for CO_2 electroreduction in [Bmim]BF_4/acetonitrile.[98] The FE of CH_3OH was up to 71.2% and the total current density reached 12.1 mA cm^{-2}. They found that IL played a crucial role in CO_2 reduction with the stabilization of $CO_2^{\bullet-}$. The synergistic effect of Mo and Bi favors the generation of CH_3OH (Figure 8A). The flowerlike In_2S_3 was synthesized as an efficient electrocatalyst for CO_2 reduction to $HCOO^-$ in IL-based electrolyte.[99] The excellent catalytic activity was attributed to the special structure and large adsorption energy of intermediate COO* and OCHO*. In addition, a defective indium selenide on carbon paper (γ-In_2Se_3/CP) was also prepared for syngas synthesis from CO_2 reduction.[100] Variation in the content of [Bmim]PF_6 and H_2O in the electrolyte can adjust the CO/H_2 ratio in a wide range (Figures 8B and 8C). WSe_2 nanoflakes (NFs) was prepared for CO_2 electroreduction to CO in 50 vol % [Emim]BF_4/H_2O solution.[101] Compared with other cathodes, the current density, FE, and TOF of producing CO were all superior at lower overpotentials (Figures 8D–8G). The IL was vital for this reaction because the cations of IL can form a complex with CO_2 to accelerate the transportation of CO_2. Cu selenide nanocatalysts can convert CO_2 to CH_3OH at low overpotential in [Bmim]PF_6 (30 wt %)/acetonitrile-H_2O solution.[102] The outstanding performance mainly comes from the excellent cooperative effect of Cu and Se in the catalysts. In addition, in [Bmim]BF_4-H_2O electrolyte, $MoTe_2$ could also be used as a catalyst for CO_2 reduction to CH_4 with high FE of 83%.[103]

Metal-Free Catalysts. Metal-free catalysts can also act as potential electrocatalysts for CO_2 reduction in IL-based electrolytes. According to a previous report, they have many intrinsic advantages that can enhance the performance of the reaction, such as excellent conductivity, high surface area, outstanding mechanical strength, and remarkable chemical stability. In addition, they are low cost and easily available in huge quantities. Although pure carbon nanocatalysts show low activity, heteroatoms can be easily introduced to adjust the chemical state and structure of the nanocatalysts to manipulate the active sites for CO_2 reduction. Combining with IL, metal-free nanocatalysts are promising electrocatalysts. The catalytic performance of carbon nanofibers (CNFs) was explored in [Emim]BF_4 and H_2O mixture electrolytes.[104] In this system, CO_2 could be reduced to CO with high current density and low overpotential. The addition of H_2O can instantly change the pH and viscosity of IL. The decrease in pH mainly originates from the generation of hydroxyl ions due to the hydrolysis of IL, which can promote the

Review

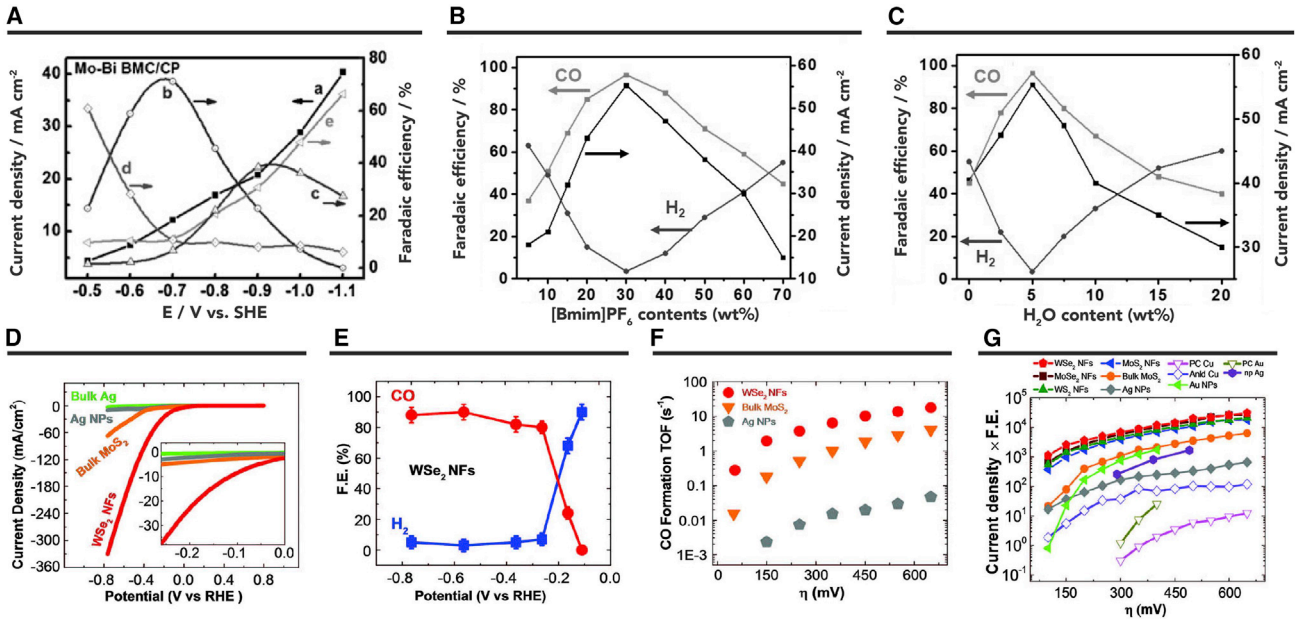

Figure 8 The Catalystic Performance of Different Metal Chalcogenides in IL-Based Electrolytes

(A) The current density and FE of the products at different applied potentials over Mo-Bi BMC/CP catalyst with a Mo:Bi molar ratio of 1:1. Reproduced with permission from Sun et al.[98] Copyright 2016, Wiley Publishers.

(B and C) FE of CO and H_2 and current density using $[Bmim]PF_6/CH_3CN/H_2O$ electrolyte with different (B) $[Bmim]PF_6$ and (C) H_2O contents over F-γ-In_2Se_3/CP catalysts. Electrolysis experiments were carried out at −2.0 V versus SCE for 5 h. Data were obtained at ambient temperature and pressure with CO_2 stream of 5 sccm. Reproduced with permission from Yang et al.[100] Copyright 2020, Wiley Publishers. CO_2 reduction performance of the TMDC catalysts, Ag NPs, and bulk Ag in the $[Emim]BF_4$ solution.

(D) CV curves for WSe_2 NFs, bulk MoS_2, Ag nanoparticles (Ag NPs), and bulk Ag in a CO_2 environment. Inset shows the current densities in low overpotentials.

(E) CO and H_2 overall FE at different applied potentials for WSe_2 NFs. The error bars represent the SD of four measurements.

(F) CO formation TOF of WSe_2 NFs, bulk MoS_2, and Ag NPs in IL-based electrolyte at overpotentials of 54–650 mV. At 54 mV overpotential, the result for Ag NPs is zero.

(G) Overview of the performance of different catalysts at different overpotentials. All TMDC and Ag NP data were obtained from chronoamperometry experiments under identical conditions. Reproduced with permission from Asadi et al.[101] Copyright 2016, AAAS Publishers.

proton concentration and then improve the rate of CO_2 reduction. It was reported that N-doped carbon (graphene-like) catalysts were efficient for the electrochemical reduction of CO_2 when using IL as the promoter.[105] The FE of CH_4 could be as high as 93.5%, and the current density was 1.4 $mA \cdot cm^{-2}$ in $[Bmim]BF_4/H_2O$ electrolyte.

Electrolyte Effects

Comparison of IL, Aqueous Electrolytes, and Organic Electrolytes

In aqueous electrolyte, the solubility of CO_2 is only 0.033 mol^{-1} under ambient conditions (298 K, 1 atm), which leads to low conversion efficiency of CO_2 reduction. Therefore, the sluggish kinetics due to the formation of $CO_2^{\cdot -}$ radical is the main energy barrier for the reaction. Consequently, adequate large overpotentials are usually required to drive this reaction.[28,35] The other complicating factor is the HER, which is prevalent in aqueous media. As a competitive reaction, it can reduce the selectivity of the desired product. Moreover, most studies focus on weakly acidic or alkaline CO_2-saturated aqueous solutions consisting of inorganic salts (e.g., anions, HCO_3^-, SO_4^{2-} Cl^-, Br^-, I^-; alkali metal cations, K^+ and Na^+) and the catalytic activity and product selectivity

Table 4. Products Formed by Bulk Electrolysis of CO_2 at an Ag Cathode in Acetonitrile (0.1 M n-Bu_4NPF_6)

Additives	$E_{applied}$ (V) versus Fc/Fc^+	Charge ©	FE (%) H_2	CO	$C_2O_4^{2-}$	HCO_2^-
Without IL[a]	−2.6[b]	12.5	0.2	53.9	39.3	0.8
2.0 mM $[C_{10}mim]BF_4$[a]	−2.3	28.5	0	45.1	53.4	0.4
2.0 mM $[C_4mpyrd]BF_4$[a]	−2.3	50.1	0	66.4	28.4	0.8
Without IL + 1.0% H_2O	−2.3	15.3	87.4	9.5	3.5	
2.0 mM $[C_{10}mim]BF_4$ + 1.0% H_2O	−2.3	61.8	1.8	70.4	27.1	0.4
2.0 mM $[C_4mpyrd]BF_4$ + 1.0% H_2O	−2.3	50.2	0.4	58.4	42.6	0.8

Reproduced with permission from Zhu et al.[56] Copyright 2016, ACS Publishers.
[a]H_2O content: 5.0 mM.
[b]This more negative potential was chosen to achieve a reduction rate that is comparable with that found in the presence of IL additive.

are enhanced even though the exact mechanism is still under debate.[28] Although there are still difficult issues with CO_2 reduction, CO_2 in aqueous electrolyte could undergo C–C coupling and be further reduced to multi-carbon products. Therefore, designing efficient catalysts for CO_2 electroreduction in aqueous electrolytes can enhance the product selectivity and diversity of the product.[28]

In organic electrolytes, the increased solubility of CO_2 is accompanied by the poor conductivity of the electrolyte.[28] At the same time, the volatilization of a large number of organic solvents also causes environmental problems. Therefore, organic solvent systems are mainly used in homogeneous catalysis or in the design of mixed electrolyte systems.

Compared with aqueous and organic electrolytes, ILs exhibit excellent activity in the electroreduction of CO_2.[28,32] They provide a medium for CO_2 reduction, and their strong absorption capacity of CO_2 promotes the reduction reaction effectively. More importantly, they can significantly increase the selectivity of products and inhibit the HER.[32] However, a large proportion of ILs are expensive and have high viscosity. Therefore, synthesizing functionalized ILs with low viscosity, high CO_2 absorption, and excellent stability is vital for CO_2 reduction. In addition, most of the catalysts currently developed can only reduce CO_2 to C1 product in IL-based electrolytes. This indicates that the reaction pathways in IL-based electrolyte are different from those in aqueous media. Therefore, it is also necessary to further study the mechanisms in IL-based electrolyte and design novel IL-based systems with high activity for multi-carbon products.

Cation and Anion Effect of ILs

Although many ILs are widely used, the promotion effect of the electrolyte remains unclear. To date, only a few studies have reported the electrolyte effect. This section discusses the recent progress in CO_2 reduction systems concerning the cation and anion effect.

Cation Effect. Imidazolium cations have unique properties in CO_2 reduction. In a recent study, Zhang et al.[56] studied the CO_2 reduction performance on an Ag electrode in acetonitrile solutions (0.1 M $[Bu_4N]PF_6$ as supporting electrolyte) containing 2.0 mM imidazolium, pyrrolidium, ammonium, phosphonium, or (trimethylamine)-(dimethylethylamine)-dihydroborate cations. They found that all these cations can enhance the kinetics of the reaction, but imidazolium and pyrrolidium are the most effective (Table 4). Rosenthal et al.[66] found that the cation in ILs can change the selectivity of products over a Bi/IL interface (Figure 6C). Selectively, CO was the main product in $[Bmim]PF_6$, and the FE for $HCOO^-$ was higher in $[DBU\text{-}H]PF_6$ (DBU, 1,8-diazobicyclo[5.4.0]undec-7-ene). These results indicated the interaction among the cation, catalyst, and CO_2 plays an important role in the electroreduction of CO_2. In addition, it was also reported that ILs with different imidazole rings had a vital influence on the catalytic activity of CO_2 electroreduction.[90] The hydrophobicity of ILs, which can be varied by the side cation chain length, was closely related to the solubility of CO_2. At the same time, the stability of the imidazole ring-CO_2 complex formed during CO_2 reduction may be decreased by the steric bulkiness with increasing side chain length. Recently, Deng et al.[106] used surface tension measurements and SFG spectroscopy to investigate the surface behavior at a liquid-air interface of 1-butyl-3-methylimidazolium methylsulfate ([Bmim]MS) aqueous solution.

Review

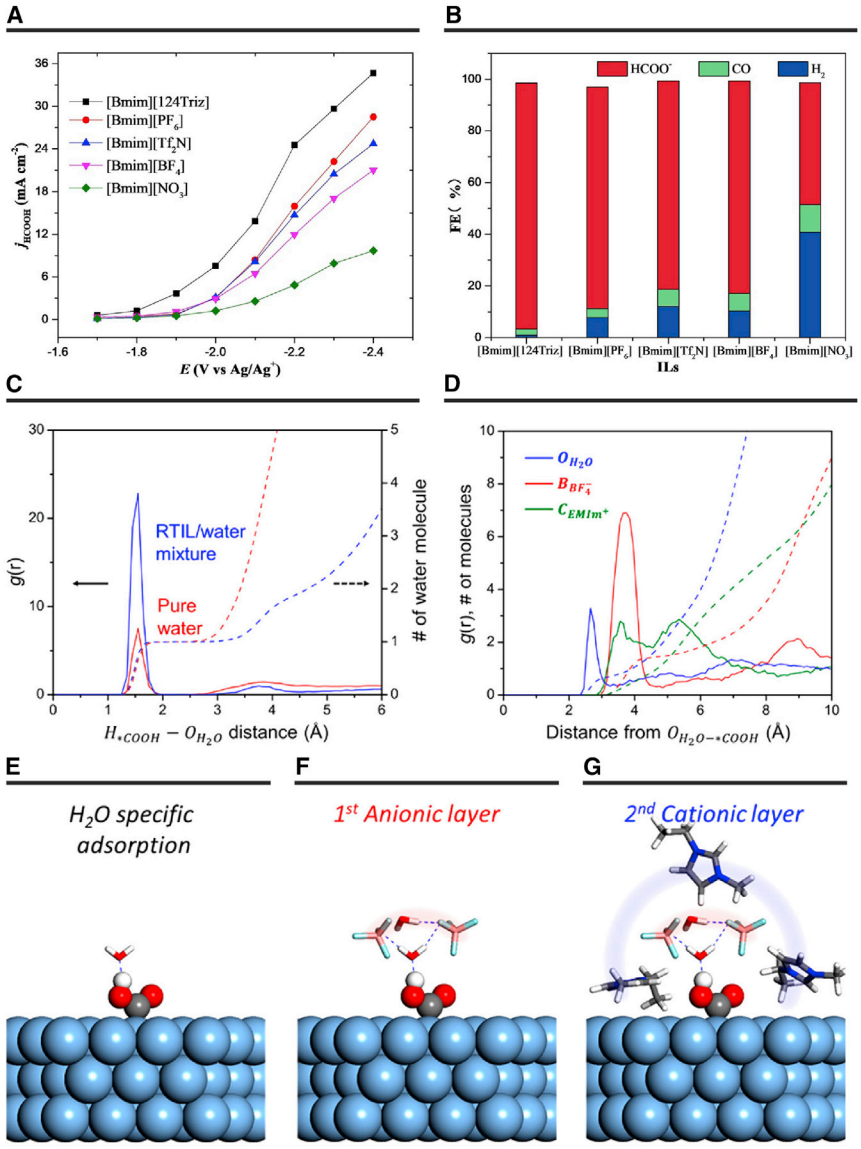

Figure 9 CO_2 Electroreduction Performances

(A) Partial current of HCOOH on the Pb catalyst.

(B) Corresponding FE for HCOOH, CO, and H_2 in IL/acetonitrile-H_2O (5 wt %). Reproduced with permission from Feng et al.[72] Copyright 2018 Wiley Publishers. Structural characteristics of the 20:80 [Emim]BF_4/H_2O mixed electrolyte surrounding the *COOH state.

(C) Calculated radial distribution functions between the hydrogen atom in *COOH and the oxygen atoms in H_2O under aqueous and mixed electrolyte conditions.

(D) Calculated radial distribution functions between the oxygen atoms in the adsorbed H_2O molecules on *COOH and the oxygen, boron, and carbon atoms in H_2O, BF_4^-, and $[Emim]^+$ in the mixed electrolyte.

(E–G) Different constituents of the mixed electrolyte form alternating layers to solvate the *COOH intermediate. (E) H_2O specific adsorption; (F) first anionic layer; (G) second cationic layer. Reproduced with permission from Lim et al.[108] Copyright 2018, ACS Publisher.

The results illustrated that the surface tension was mainly affected by the cations in ILs. Consistently, Dyson et al.[45] also pointed out that different imidazolium rings are vital for efficient CO_2 reduction (Figure 5D).

Anion Effect. Anions in the imidazolium-based ILs also affect CO_2 reduction. Zhang et al.[72] built an ionic microhabitat composed of an anion-functionalized IL [Bmim]124Triz, acetonitrile, and H_2O for CO_2 electroreduction. Other ILs with different anions, such as BF_4^-, PF_6^-, NO_3^-, and NTF_2^-, were used for comparison. The authors found that [Bmim]124Triz promotes the solubility of CO_2 and bending linear CO_2 by forming the [124Triz]-CO_2 adduct. The activated CO_2 can be transferred into the catalyst surface easily, which can increase the generation of the target product (Figures 9A and 9B). They also used computational results to validate the underlying mechanism of the super-basic IL. Interestingly, they found the bond length in [Bmim]$\cdots CO_2 \cdots$124Triz (2.30 Å) was much shorter than that in other imidazolium-based ILs: [Bmim]PF_6 (3.15 Å), [Bmim]BF_4 (2.93 Å), [Bmim]NTF_2 (3.08 Å), and [Bmim]NO_3 (3.29 Å). This indicated that the interaction between CO_2 and [Bmim]124Triz is much stronger than that between the CO_2 and the other ILs. Therefore, the fast transportation feasibility of activated CO_2 to the catalyst surface led to higher FE of HCOOH.

The comprehensive effect of cation and anion was also investigated by Compton et al.[107] They pointed out that the cation bound to the Ag surface allowed the CO_2 molecule to access the Ag surface before the process of desorption and an irreversible reduction of CO_2. In addition, the anions in ILs may affect the local solvent structure other than the solubility of CO_2. The electric double layer adjacent to the Ag surface can be occupied by cations and anions and allow CO_2 transport to the Ag surface before electron transfer occurs. Based on previous reports, we can summarize that the cations and anions in ILs play important roles in CO_2 electroreduction. They can interact with the reaction intermediates or change the properties of the electric double layer adjacent to the catalyst surface.

Mechanism

In general, the CO_2 electroreduction process is driven in imidazolium-based ILs. The importance of the effect of ILs on the activity toward CO_2 reduction was investigated by Lim et al.[108]. In this work, the authors presented a combined experimental and theoretical study to investigate the promotion effect of ILs. Contrary to the previous concept, which assumed specific intermolecular coordination by ILs with the reaction intermediate, the authors figured out that the promotion effect was manifested by changing the reaction microenvironment. They found that the local coordinating environment of *COOH was nearly identical for aqueous and [Emim]BF_4/H_2O systems. A single H_2O molecule bound to *COOH through a hydrogen bond (Figures 9C and 9E). However, considering that the H_2O molecule served as a primary proton source, the local atomic geometry was responsible for the facile proton transfer.

In [Emim]BF_4/H_2O electrolyte, approximately one or two H_2O and BF_4^- molecules were closed to the adsorbed H_2O molecule. Then, four $[Emim]^+$ molecules surrounded an H_2O-BF_4^- complex via a strong cation-anion attraction (Figures 9D, 9F, and 9G). The combination of these complex noncovalent interactions in the mixed electrolytes formed an exotic microenvironment for *COOH with an alternating solvation shell structure. These three-dimensional atomic arrangements can result in $[Emim]^+$ being in direct contact with the catalyst surface, surrounded by the key reaction intermediate. This phenomenon results in a significant polarization of the electron density on the catalyst surface. Then, plenty of metal electrons can be polarized toward the *COOH intermediate, which induces a strong local field effect at the catalyst interface and stabilizes the *COOH intermediate. Therefore, the electrical double-layer interface provided a suitable microenvironment for solvating the intermediate, which can be well preserved with the variations in chemical details because the solvation energy is dominated by the nonspecific interaction.

To further understand the CO_2 electroreduction pathway, Nakamura et al.[109] figured out the possible intermediates and the transition states from CO_2 to CO in [Emim]BF_4 electrolyte. They stressed that the complex [Emim-COOH] generated during the reaction can be decomposed to CO. In the reaction pathway, H_2O was a co-catalyst to facilitate proton transfer. The pathway to CO was thermodynamically more favored than that to HCOOH in IL-based electrolyte. As shown in Figure 10, there are many reaction pathways from [Emim]BF_4 and CO_2 to the final product CO. The thermodynamically favorable paths are marked by green arrows and unfavorable ones by red arrows. The black arrows represent the electron transfer from the electrodes. Although important progress has been made in electroreduction of CO_2 with IL-based electrolyte, research on the mechanism is still in its infancy, especially on understanding of the interaction between the liquid medium and the catalyst surface, which is important for the systematic design of efficient catalytic systems.

Perspective

ILs have shown promising applications in electroreduction of CO_2 due to their unique properties. To date, significant progress has been achieved in this interesting area. However, some related issues need to be solved.

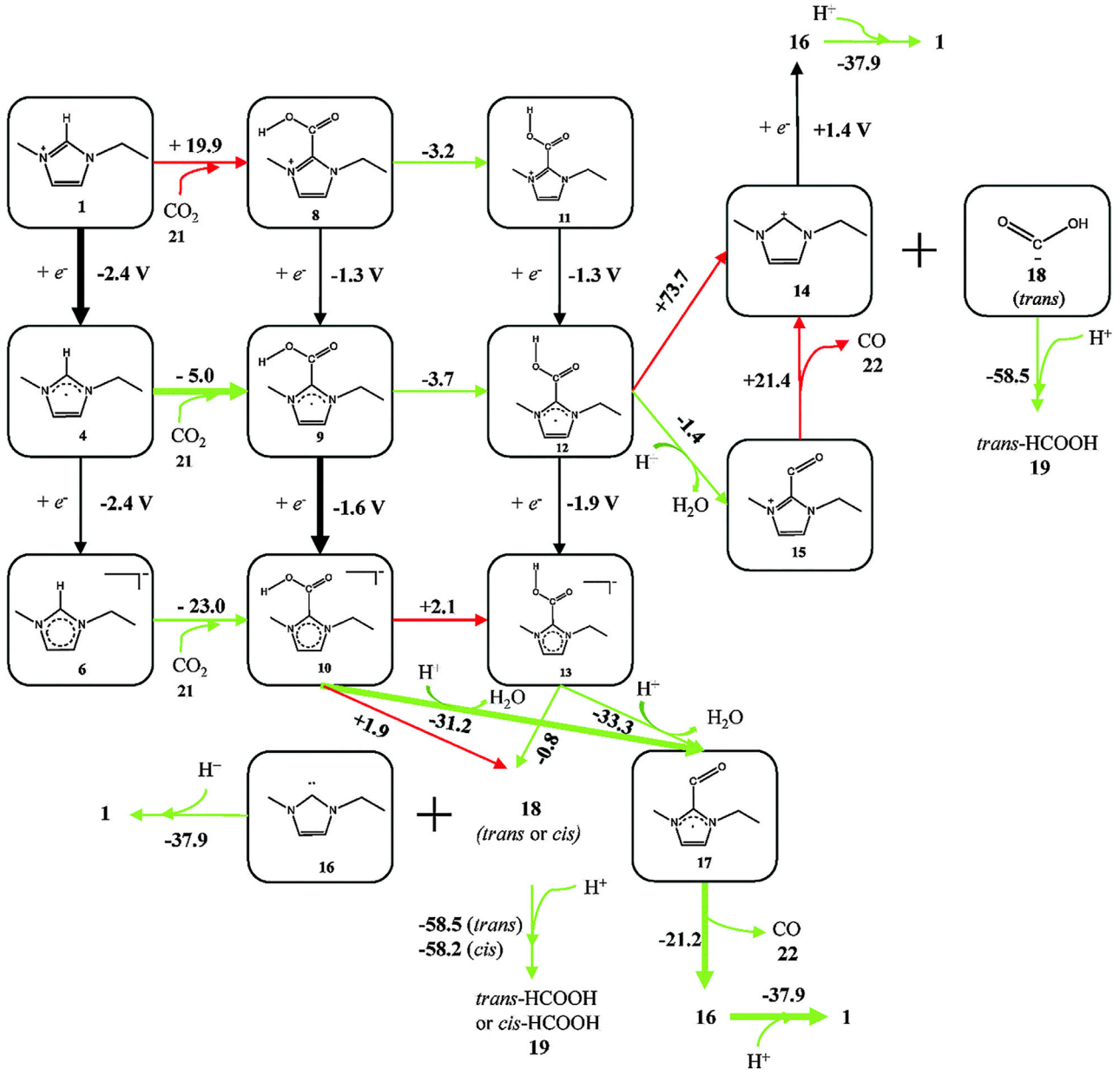

Figure 10 A Schematic Flow of Reaction Intermediates

Reproduced with permission from Wang et al.[109] Copyright 2015, RSC Publisher.

(1) For IL-based electrolyte, large-scale application of CO_2 electroreduction has not been realized. On the one hand, the current density at high FE of the desired product is still low for industrial applications (a few hundred mA cm^{-2} for industrial level[110]). On the other hand, the high cost and high viscosity of ILs are also crucial factors to inhibit its large-scale application. Therefore, highly active, selective, and stable catalyst-electrolyte systems should be explored to promote commercial application, especially using renewable electricity. The design of novel electrochemical devices such as flow cells and gas-diffusion electrodes can overcome the poor mass transferability and increase the current density. Moreover, synthesizing functionalized ILs with low viscosity, high CO_2 absorption, and excellent stability can enhance the capacity of activating CO_2 molecules and achieve multiple reuse of the electrolyte.

(2) Up to now, most of the catalysts that have been developed can only reduce CO_2 to C1 products in IL-based electrolytes. The current density and FE for producing various products with two or more carbons are still not satisfactory because C–C coupling is involved. Therefore, it is interesting and important to explore novel catalyst-electrolyte systems with high activity for C–C coupling. Excellent catalysts with high potentials for the HER should be designed that can combine with ILs to provide a good three-phase contact interface for enhancing the selectivity toward multi-carbon products. While the electrocatalytic reduction of CO_2 and H_2O to produce valuable chemicals and fuels is of great importance, much attention should be given to investigations about new electrocatalytic reactions of CO_2 and organic compounds to synthesize more valuable chemicals. IL-based electrolytes may be more advantageous for this kind of reaction because ILs can dissolve both CO_2 and organic substances. Moreover, the interaction among ILs, CO_2, and organic reactants can be tuned by changing the structure of the IL, which may enhance catalytic activity and FE for a product, and even control the reaction pathways.

(3) The interfacial properties and the mechanisms in IL-based electrolytes are still unclear. To further understand CO_2 reduction in IL-based electrolytes, comprehensive recognition of the theoretical and experimental mechanisms is needed. An in-depth study should also be carried out on the role of cations and anions in ILs and the microscopic mechanism of proton-electron transport and transfer. It is expected that combining *in situ* techniques with theoretical calculations can be used to address this issue.

Based on the above discussion, CO_2 electroreduction in IL-based electrolytes can be used to produce many value-added chemicals and feedstocks for fuels. The design of functionalized, low-toxicity, and easily prepared ILs will have broad application in CO_2 electroreduction. Although exploring efficient catalyst-electrolyte systems for CO_2 electroreduction is challenging, it should be given much attention because it is crucial for the development of this area.

Acknowledgments

The work was supported financially by the National Key Research and Development Program of China (2017YFA0403102), National Natural Science Foundation of China (21773267, 21890761, 21533011), and the Chinese Academy of Sciences (QYZDY-SSW-SLH013).

Declaration of interests

The authors declare no competing interests.

References

1. He, M., Sun, Y., and Han, B. (2013). Green carbon science: scientific basis for integrating carbon resource processing, utilization, and recycling. Angew. Chem. Int. Ed. *52*, 9620–9633.

2. Klankermayer, J., Wesselbaum, S., Beydoun, K., and Leitner, W. (2016). Selective catalytic synthesis using the combination of carbon dioxide and hydrogen: catalytic chess at the interface of energy and chemistry. Angew. Chem. Int. Ed. *55*, 7296–7343.

3. Tu, W., Zhou, Y., and Zou, Z. (2014). Photocatalytic conversion of CO_2 into renewable hydrocarbon fuels: state-of-the-art accomplishment, challenges, and prospects. Adv. Mater. *26*, 4607–4626.

4. Sun, Z., Ma, T., Tao, H., Fan, Q., and Han, B. (2017). Fundamentals and challenges of electrochemical CO_2 reduction using two-dimensional materials. Chem *3*, 560–587.

5. Vasileff, A., Zheng, Y., and Qiao, S. (2017). Carbon solving carbon's problems: recent progress of nanostructured carbon-based catalysts for the electrochemical reduction of CO_2. Adv. Energy Mater. *7*, 1700759.

6. Li, Y., and Sun, Q. (2016). Recent advances in breaking scaling relations for effective electrochemical conversion of CO_2. Adv. Energy Mater. *6*, 1600463.

7. Ross, M.B., De Luna, P., Li, Y., Dinh, C.T., Kim, D., Yang, P., and Sargent, E.H. (2019). Designing materials

for electrochemical carbon dioxide recycling. Nat. Catal. *2*, 648–658.

8. Bai, X., Chen, W., Zhao, C., Li, S., Song, Y., Ge, R., Wei, W., and Sun, Y. (2017). Exclusive formation of formic acid from CO_2 electroreduction by a tunable Pd-Sn alloy. Angew. Chem. Int. Ed. *129*, 12387–12391.

9. Song, Y., Chen, W., Zhao, C., Li, S., Wei, W., and Sun, Y. (2017). Metal-free nitrogen-doped mesoporous carbon for electroreduction of CO_2 to ethanol. Angew. Chem. Int. Ed. *56*, 10840–10844.

10. Yang, H., Qin, S., Wang, H., and Lu, J. (2015). Organically doped palladium: a highly efficient catalyst for electroreduction of CO_2 to methanol. Green Chem. *17*, 5144–5148.

11. Lan, Y., Gai, C., Kenis, P.J.A., and Lu, J. (2014). Electrochemical reduction of carbon dioxide on Cu/CuO core/shell catalysts. ChemElectroChem *1*, 1577–1582.

12. Zhang, L., Zhao, Z., and Gong, J. (2017). Nanostructured materials for heterogeneous electrocatalytic CO_2 reduction and their related reaction mechanisms. Angew. Chem. Int. Ed. *56*, 11326–11353.

13. Deng, W., Zhang, L., Li, L., Chen, S., Hu, C., Zhao, Z., Wang, T., and Gong, J. (2019). Crucial role of surface hydroxyls on the activity and stability in electrochemical CO_2 reduction. J. Am. Chem. Soc. *141*, 2911–2915.

14. Ding, C., Li, A., Lu, S.M., Zhang, H., and Li, C. (2016). In situ electrodeposited indium nanocrystals for efficient CO_2 reduction to CO with low overpotential. ACS Catal. *6*, 6438–6443.

15. De Luna, P., Quintero-Bermudez, R., Dinh, C.T., Ross, M.B., Bushuyev, O.S., Todorović, P., Regier, T., Kelley, S.O., Yang, P., and Sargent, E.H. (2018). Catalyst electroredeposition controls morphology and oxidation state for selective carbon dioxide reduction. Nat. Catal. *1*, 103–110.

16. Yin, Z., Palmore, G.T.R., and Sun, S. (2019). Electrochemical reduction of CO_2 catalyzed by metal nanocatalysts. Trends Chem. *1*, 739–750.

17. Fan, Q., Hou, P., Choi, C., Wu, T., Hong, S., Li, F., Soo, Y.L., Kang, P., Jung, Y., and Sun, Z. (2020). Activation of Ni particles into single Ni-N atoms for efficient electrochemical reduction of CO_2. Adv. Energy Mater. *10*, 1903068.

18. Gao, D., Zhou, H., Wang, J., Miao, S., Yang, F., Wang, G., Wang, J., and Bao, X. (2015). Size-dependent electrocatalytic reduction of CO_2 over Pd nanoparticles. J. Am. Chem. Soc. *137*, 4288–4291.

19. Gao, S., Lin, Y., Jiao, X., Sun, Y., Luo, Q., Zhang, W., Li, D., Yang, J., and Xie, Y. (2016). Partially oxidized atomic cobalt layers for carbon dioxide electroreduction to liquid fuel. Nature *529*, 68–71.

20. Zhang, A., He, R., Li, H., Chen, Y., Kong, T., Li, K., Ju, H., Zhu, J., Zhu, W., and Zeng, J. (2018). Nickel doping in atomically thin tin disulfide nanosheets enables highly efficient CO_2 reduction. Angew. Chem. Int. Ed. *130*, 11120–11124.

21. Li, F., Chen, L., Knowles, G.P., MacFarlane, D.R., and Zhang, J. (2017). Hierarchical mesoporous SnO_2 nanosheets on carbon cloth: a robust and flexible electrocatalyst for CO_2 reduction with high efficiency and selectivity. Angew. Chem. Int. Ed. *56*, 505–509.

22. Yang, H., Wu, Y., Li, G., Lin, Q., Hu, Q., Zhang, Q., Liu, J., and He, C. (2019). Scalable production of efficient single-atom copper decorated carbon membranes for CO_2 electroreduction to methanol. J. Am. Chem. Soc. *141*, 12717–12723.

23. Shen, J., Kortlever, R., Kas, R., Birdja, Y.Y., Diaz-Morales, O., Kwon, Y., Ledezma-Yanez, I., Schouten, K.J.P., Mul, G., and Koper, M.T. (2015). Electrocatalytic reduction of carbon dioxide to carbon monoxide and methane at an immobilized cobalt protoporphyrin. Nat. Commun. *6*, 8177.

24. Varela, A.S., Ranjbar Sahraie, N., Steinberg, J., Ju, W., Oh, H.-S., and Strasser, P. (2015). Metal-doped nitrogenated carbon as an efficient catalyst for direct CO_2 electroreduction to CO and hydrocarbons. Angew. Chem. Int. Ed. *54*, 10758–10762.

25. Lum, Y., and Ager, J.W. (2019). Evidence for product-specific active sites on oxide-derived Cu catalysts for electrochemical CO_2 reduction. Nat. Catal. *2*, 86–93.

26. Singh, M.R., Kwon, Y., Lum, Y., Ager, J.W., and Bell, A.T. (2016). Hydrolysis of electrolyte cations enhances the electrochemical reduction of CO_2 over Ag and Cu. J. Am. Chem. Soc. *138*, 13006–13012.

27. Weng, Z., Wu, Y., Wang, M., Jiang, J., Yang, K., Huo, S., Wang, X., Ma, Q., Brudvig, G.W., Batista, V.S., et al. (2018).

Active sites of copper-complex catalytic materials for electrochemical carbon dioxide reduction. Nat. Commun. *9*, 415.

28. Moura de Salles Pupo, M., and Kortlever, R. (2019). Electrolyte effects on the electrochemical reduction of CO_2. ChemPhysChem *20*, 2926–2935.

29. Yang, W., Dastafkan, K., Jia, C., and Zhao, C. (2018). Design of electrocatalysts and electrochemical cells for carbon dioxide reduction reactions. Adv. Mater. Technol. *3*, 1700377.

30. Gunawan, C.A., Ge, M., and Zhao, C. (2014). Robust and versatile ionic liquid microarrays achieved by microcontact printing. Nat. Commun. *5*, 3744.

31. Lu, W., Jia, B., Cui, B., Zhang, Y., Yao, K., Zhao, Y., and Wang, J. (2017). Efficient photoelectrochemical reduction of carbon dioxide to formic acid: a functionalized ionic liquid as an absorbent and electrolyte. Angew. Chem. Int. Ed. *56*, 11851–11854.

32. Feng, J., Zeng, S., Feng, J., Dong, H., and Zhang, X. (2018). CO_2 electroreduction in ionic liquids: a review. Chin. J. Chem. .. *36*, 961–970.

33. MacFarlane, D.R., Forsyth, M., Howlett, P.C., Pringle, J.M., Sun, J., Annat, G., Neil, W., and Izgorodina, E.I. (2007). Ionic liquids in electrochemical devices and processes: managing interfacial electrochemistry. Acc. Chem. Res. *40*, 1165–1173.

34. Vedharathinam, V., Qi, Z., Horwood, C., Bourcier, B., Stadermann, M., Biener, J., and Biener, M. (2019). Using a 3D porous flow-through electrode geometry for high-rate electrochemical reduction of CO_2 to CO in ionic liquid. ACS Catal. *9*, 10605–10611.

35. Zhang, W., Hu, Y., Ma, L., Zhu, G., Wang, Y., Xue, X., Chen, R., Yang, S., and Jin, Z. (2018). Progress and perspective of electrocatalytic CO_2 reduction for renewable carbonaceous fuels and chemicals. Adv. Sci. *5*, 1700275.

36. Rosen, B.A., Salehi-Khojin, A., Thorson, M.R., Zhu, W., Whipple, D.T., Kenis, P.J., and Masel, R.I. (2011). Ionic liquid-mediated selective conversion of CO_2 to CO at low overpotentials. Science *334*, 643–644.

37. Rees, N.V., and Compton, R.G. (2011). Electrochemical CO_2 sequestration in ionic liquids; a perspective. Energ. Environ. Sci. *4*, 403–408.

38. Lim, H.K., and Kim, H. (2017). The mechanism of room-temperature ionic-liquid-based electrochemical CO_2 reduction: a review. Molecules *22*, 536.

39. Benson, E.E., Kubiak, C.P., Sathrum, A.J., and Smieja, J.M. (2009). Electrocatalytic and homogeneous approaches to conversion of CO_2 to liquid fuels. Chem. Soc. Rev. *38*, 89–99.

40. Grills, D.C., Matsubara, Y., Kuwahara, Y., Golisz, S.R., Kurtz, D.A., and Mello, B.A. (2014). Electrocatalytic CO_2 reduction with a homogeneous catalyst in ionic liquid: high catalytic activity at low overpotential. J. Phys. Chem. Lett. *5*, 2033–2038.

41. Choi, J., Benedetti, T.M., Jalili, R., Walker, A., Wallace, G.G., and Officer, D.L. (2016). High performance Fe porphyrin/ionic liquid Co-catalyst for electrochemical CO_2 reduction. Chem. Eur. J. *22*, 14158–14161.

42. Honores, J., Quezada, D., García, M., Calfumán, K., Muena, J.P., Aguirre, M.J., Arévalo, M.C., and Isaacs, M. (2017). Carbon neutral electrochemical conversion of carbon dioxide mediated by $[Mn^{+}$(cyclam)Cln] (M = Ni^{2+} and Co^{3+}) on mercury free electrodes and ionic liquids as reaction media. Green Chem. *19*, 1155–1162.

43. Rosen, B.A., Haan, J.L., Mukherjee, P., Braunschweig, B., Zhu, W., Salehi-Khojin, A., Dlott, D.D., and Masel, R.I. (2012). In situ spectroscopic examination of a low overpotential pathway for carbon dioxide conversion to carbon monoxide. J. Phys. Chem. C *116*, 15307–15312.

44. García Rey, N., and Dlott, D.D. (2015). Structural transition in an ionic liquid controls CO_2 electrochemical reduction. J. Phys. Chem. C *119*, 20892–20899.

45. Lau, G.P., Schreier, M., Vasilyev, D., Scopelliti, R., Grätzel, M., and Dyson, P.J. (2016). New insights into the role of imidazolium-based promoters for the electroreduction of CO_2 on a silver electrode. J. Am. Chem. Soc. *138*, 7820–7823.

46. Hollingsworth, N., Taylor, S.R., Galante, M.T., Jacquemin, J., Longo, C., Holt, K.B., de Leeuw, N.H., and Hardacre, C. (2015). Reduction of carbon dioxide to formate at low overpotential using a superbase ionic liquid. Angew. Chem. Int. Ed. *54*, 14164–14168.

47. Zhu, W., Michalsky, R., Metin, Ö., Lv, H., Guo, S., Wright, C.J., Sun, X., Peterson, A.A., and Sun, S. (2013). Monodisperse Au nanoparticles for selective

electrocatalytic reduction of CO_2 to CO. J. Am. Chem. Soc. *135*, 16833–16836.

48. Yang, D., Li, Q., Shen, F., Wang, Q., Li, L., Song, N., Dai, Y., and Shi, J. (2016). Electrochemical impedance studies of CO_2 reduction in ionic liquid/organic solvent electrolyte on Au electrode. Electrochim. Acta *189*, 32–37.

49. Papasizza, M., and Cuesta, A. (2018). In situ monitoring using ATR-SEIRAS of the electrocatalytic reduction of CO_2 on Au in an ionic liquid/water mixture. ACS Catal. *8*, 6345–6352.

50. Fu, Y., Ehrenburg, M.R., Broekmann, P., and Rudnev, A.V. (2018). Surface structure sensitivity of CO_2 electroreduction on low-index gold single crystal electrodes in ionic liquids. ChemElectroChem *5*, 748–752.

51. Martindale, B.C., and Compton, R.G. (2012). Formic acid electro-synthesis from carbon dioxide in a room temperature ionic liquid. Chem. Commun. *48*, 6487–6489.

52. Bruzon, D.A., Tiongson, J.K., Tapang, G., and Martinez, I.S. (2017). Electroreduction and solubility of CO_2 in methoxy-and nitrile-functionalized imidazolium (FAP) ionic liquids. J. Appl. Electrochem. *47*, 1251–1260.

53. Hanc-Scherer, F.A., Montiel, M.A., Montiel, V., Herrero, E., and Sánchez-Sánchez, C.M. (2015). Surface structured platinum electrodes for the electrochemical reduction of carbon dioxide in imidazolium based ionic liquids. Phys. Chem. Chem. Phys. *17*, 23909–23916.

54. Salehi-Khojin, A., Jhong, H.R.M., Rosen, B.A., Zhu, W., Ma, S., Kenis, P.J., and Masel, R.I. (2013). Nanoparticle silver catalysts that show enhanced activity for carbon dioxide electrolysis. J. Phys. Chem. C *117*, 1627–1632.

55. Neubauer, S.S., Krause, R.K., Schmid, B., Guldi, D.M., and Schmid, G. (2016). Overpotentials and faraday efficiencies in CO_2 electrocatalysis-the impact of 1-ethyl-3-methylimidazolium trifluoromethanesulfonate. Adv. Energy Mater. *6*, 1502231.

56. Zhao, S., Horne, M., Bond, A.M., and Zhang, J. (2016). Is the imidazolium cation a unique promoter for electrocatalytic reduction of carbon dioxide? J. Phys. Chem. C *120*, 23989–24001.

57. Rudnev, A.V., Fu, Y., Gjuroski, I., Stricker, F., Furrer, J., Kovács, N., Vesztergom, S., and Broekmann, P. (2017). Transport matters: boosting CO_2 electroreduction in mixtures of [Bmim][BF_4]/water by enhanced diffusion. ChemPhysChem *18*, 3153–3162.

58. Rudnev, A.V., Kiran, K., Cedeño López, A., Dutta, A., Gjuroski, I., Furrer, J., and Broekmann, P. (2019). Enhanced electrocatalytic CO formation from CO_2 on nanostructured silver foam electrodes in ionic liquid/water mixtures. Electrochim. Acta *306*, 245–253.

59. Vasilyev, D.V., Rudnev, A.V., Broekmann, P., and Dyson, P.J. (2019). A general and facile approach for the electrochemical reduction of carbon dioxide inspired by deep eutectic solvents. ChemSusChem *12*, 1635–1639.

60. Zhang, L., Wu, N., Zhang, J., Hu, Y., Wang, Z., Zhuang, L., and Jin, X. (2017). Imidazolium ions with an alcohol substituent for enhanced electrocatalytic reduction of CO_2. ChemSusChem *10*, 4824–4828.

61. Hollingsworth, N., Taylor, S.R., Galante, M.T., Jacquemin, J., Longo, C., Holt, K.B., de Leeuw, N.H., and Hardacre, C. (2015). CO_2 capture and electrochemical conversion using superbasic [P_{66614}][124Triz]. Faraday Discuss. *183*, 389–400.

62. Koh, J.H., Jeon, H.S., Jee, M.S., Nursanto, E.B., Lee, H., Hwang, Y.J., and Min, B.K. (2015). Oxygen plasma induced hierarchically structured gold electrocatalyst for selective reduction of carbon dioxide to carbon monoxide. J. Phys. Chem. C *119*, 883–889.

63. Gonçalves, W.D.G., Zanatta, M., Simon, N.M., Rutzen, L.M., Walsh, D.A., and Dupont, J. (2019). Efficient electrocatalytic CO_2 reduction driven by ionic liquid buffer-like solutions. ChemSusChem *12*, 4170–4175.

64. DiMeglio, J.L., and Rosenthal, J. (2013). Selective conversion of CO_2 to CO with high efficiency using an inexpensive bismuth-based electrocatalyst. J. Am. Chem. Soc. *135*, 8798–8801.

65. Medina-Ramos, J., DiMeglio, J.L., and Rosenthal, J. (2014). Efficient reduction of CO_2 to CO with high current density using in situ or ex situ prepared Bi-based materials. J. Am. Chem. Soc. *136*, 8361–8367.

66. Atifi, A., Boyce, D.W., DiMeglio, J.L., and Rosenthal, J. (2018). Directing the outcome of CO_2 reduction at

bismuth cathodes using varied ionic liquid promoters. ACS Catal. *8*, 2857–2863.

67. Zhang, Z., Chi, M., Veith, G.M., Zhang, P., Lutterman, D.A., Rosenthal, J., Overbury, S.H., Dai, S., and Zhu, H. (2016). Rational design of Bi nanoparticles for efficient electrochemical CO_2 reduction: the elucidation of size and surface condition effects. ACS Catal. *6*, 6255–6264.

68. Zhang, X., Zhao, Y., Hu, S., Gliege, M.E., Liu, Y., Liu, R., Scudiero, L., Hu, Y., and Ha, S. (2017). Electrochemical reduction of carbon dioxide to formic acid in ionic liquid [Emim][$N(CN)_2$]/water system. Electrochim. Acta *247*, 281–287.

69. Medina-Ramos, J., Pupillo, R.C., Keane, T.P., DiMeglio, J.L., and Rosenthal, J. (2015). Efficient conversion of CO_2 to CO using tin and other inexpensive and easily prepared post-transition metal catalysts. J. Am. Chem. Soc. *137*, 5021–5027.

70. Zhu, Q., Ma, J., Kang, X., Sun, X., Liu, H., Hu, J., Liu, Z., and Han, B. (2016). Efficient reduction of CO_2 into formic acid on a lead or tin electrode using an ionic liquid catholyte mixture. Angew. Chem. Int. Ed. *55*, 9012–9016.

71. Sun, L., Ramesha, G.K., Kamat, P.V., and Brennecke, J.F. (2014). Switching the reaction course of electrochemical CO_2 reduction with ionic liquids. Langmuir *30*, 6302–6308.

72. Feng, J., Zeng, S., Liu, H., Feng, J., Gao, H., Bai, L., Dong, H., Zhang, S., and Zhang, X. (2018). Insights into carbon dioxide electroreduction in ionic liquids: carbon dioxide activation and selectivity tailored by ionic microhabitat. ChemSusChem *11*, 3191–3197.

73. Wu, H., Song, J., Xie, C., Hu, Y., Ma, J., Qian, Q., and Han, B. (2018). Design of naturally derived lead phytate as an electrocatalyst for highly efficient CO_2 reduction to formic acid. Green Chem. *20*, 4602–4606.

74. Chen, L., Guo, S.X., Li, F., Bentley, C., Horne, M., Bond, A.M., and Zhang, J. (2016). Electrochemical reduction of CO_2 at metal electrodes in a distillable ionic liquid. ChemSusChem *9*, 1271–1278.

75. Medina-Ramos, J., Zhang, W., Yoon, K., Bai, P., Chemburkar, A., Tang, W., Atifi, A., Lee, S.S., Fister, T.T., Ingram, B.J., et al. (2018). Cathodic corrosion at the bismuth-ionic liquid electrolyte interface under conditions for CO_2 reduction. Chem. Mater. *30*, 2362–2373.

76. Watkins, J.D., and Bocarsly, A.B. (2014). Direct reduction of carbon dioxide to formate in high-gas-capacity ionic liquids at post-transition-metal electrodes. ChemSusChem *7*, 284–290.

77. Huan, T.N., Simon, P., Rousse, G., Génois, I., Artero, V., and Fontecave, M. (2017). Porous dendritic copper: an electrocatalyst for highly selective CO_2 reduction to formate in water/ionic liquid electrolyte. Chem. Sci. *8*, 742–747.

78. Zhu, Q., Yang, D., Liu, H., Sun, X., Chen, C., Bi, J., Liu, J., Wu, H., and Han, B. (2020). Hollow metal organic framework-mediated in-situ architecture of copper dendrites for enhanced CO_2 electroreduction. Angew. Chem. Int. Ed. https://doi.org/10.1002/anie.202001216.

79. Pardal, T., Messias, S., Sousa, M., Machado, A.S.R., Rangel, C.M., Nunes, D., Pinto, J.V., Martins, R., and da Ponte, M.N. (2017). Syngas production by electrochemical CO_2 reduction in an ionic liquid based-electrolyte. J. Co_2 Util. *18*, 62–72.

80. Lu, L., Sun, X., Ma, J., Yang, D., Wu, H., Zhang, B., Zhang, J., and Han, B. (2018). Highly efficient electroreduction of CO_2 to methanol on palladium-copper bimetallic aerogels. Angew. Chem. Int. Ed. *130*, 14345–14349.

81. Sacci, R.L., Velardo, S., Xiong, L., Lutterman, D.A., and Rosenthal, J. (2019). Copper-tin alloys for the electrocatalytic reduction of CO_2 in an imidazolium-based non-aqueous electrolyte. Energies *12*, 12.

82. Roy, N., Shibano, Y., Terashima, C., Katsumata, K.i., Nakata, K., Kondo, T., Yuasa, M., and Fujishima, A. (2016). Ionic-liquid-assisted selective and controlled electrochemical CO_2 reduction at Cu-modified boron-doped diamond electrode. ChemElectroChem *3*, 1044–1047.

83. Sun, X., Zhu, Q., Kang, X., Liu, H., Qian, Q., Ma, J., Zhang, Z., Yang, G., and Han, B. (2017). Design of a Cu (I)/C-doped boron nitride electrocatalyst for efficient conversion of CO_2 into acetic acid. Green Chem. *19*, 2086–2091.

84. Huang, P., Cheng, M., Zhang, H., Zuo, M., Xiao, C., and Xie, Y. (2019). Single Mo atom realized enhanced CO_2 electro-reduction into formate on N-doped graphene. Nano Energy *61*, 428–434.

85. Shi, J., Shao, D., Zhang, J., Tan, D., Tan, X., Zhang, B., Han, B., Zhang, F., Liu, L., and Cheng, X. (2018). Highly selective and efficient reduction of CO_2 to CO on cadmium electrodes derived from cadmium hydroxide. Chem. Commun. *54*, 5450–5453.

86. Kang, X., Zhu, Q., Sun, X., Hu, J., Zhang, J., Liu, Z., and Han, B. (2016). Highly efficient electrochemical reduction of CO_2 to CH_4 in an ionic liquid using a metal-organic framework cathode. Chem. Sci. *7*, 266–273.

87. Quezada, D., Honores, J., García, M., Armijo, F., and Isaacs, M. (2014). Electrocatalytic reduction of carbon dioxide on a cobalt tetrakis (4-aminophenyl) porphyrin modified electrode in $BmimBF_4$. New J. Chem. *38*, 3606–3612.

88. Chu, D., Qin, G., Yuan, X., Xu, M., Zheng, P., and Lu, J. (2008). Fixation of CO_2 by electrocatalytic reduction and electropolymerization in ionic liquid-H_2O solution. ChemSusChem *1*, 205–209.

89. Oh, Y., and Hu, X. (2015). Ionic liquids enhance the electrochemical CO_2 reduction catalyzed by MoO_2. Chem. Commun. *51*, 13698–13701.

90. Wu, H., Song, J., Xie, C., Hu, Y., and Han, B. (2018). Highly efficient electrochemical reduction of CO_2 into formic acid over lead dioxide in an ionic liquid-catholyte mixture. Green Chem. *20*, 1765–1769.

91. Lu, L., Sun, X., Ma, J., Zhu, Q., Wu, C., Yang, D., and Han, B. (2018). Selective electroreduction of carbon dioxide to formic acid on electrodeposited SnO_2@ N-doped porous carbon catalysts. Sci. China Chem. *61*, 228–235.

92. Jariwala, D., Sangwan, V.K., Lauhon, L.J., Marks, T.J., and Hersam, M.C. (2014). Emerging device applications for semiconducting two-dimensional transition metal dichalcogenides. ACS Nano *8*, 1102–1120.

93. Wang, H., Feng, H., and Li, J. (2014). Graphene and graphene-like layered transition metal dichalcogenides in energy conversion and storage. Small *10*, 2165–2181.

94. Wang, H., Yuan, H., Sae Hong, S., Li, Y., and Cui, Y. (2015). Physical and chemical tuning of two-dimensional transition metal dichalcogenides. Chem. Soc. Rev. *44*, 2664–2680.

95. Aljabour, A., Coskun, H., Zheng, X., Kibria, M.G., Strobel, M., Hild, S., Kehrer, M., Stifter, D., Sargent, E.H., and Stadler, P. (2020). Active sulfur sites in semimetallic titanium disulfide enable CO_2 electroreduction. ACS Catal. *10*, 66–72.

96. Asadi, M., Kumar, B., Behranginia, A., Rosen, B.A., Baskin, A., Repnin, N., Pisasale, D., Phillips, P., Zhu, W., and Haasch, R. (2014). Robust carbon dioxide reduction on molybdenum disulphide edges. Nat. Commun. *5*, 4470.

97. Lv, K., Suo, W., Shao, M., Zhu, Y., Wang, X., Feng, J., and Fang, M. (2019). Nitrogen doped MoS_2 and nitrogen doped carbon dots composite catalyst for electroreduction CO_2 to CO with high Faradaic efficiency. Nano Energy *63*, 9.

98. Sun, X., Zhu, Q., Kang, X., Liu, H., Qian, Q., Zhang, Z., and Han, B. (2016). Molybdenum-bismuth bimetallic chalcogenide nanosheets for highly efficient electrocatalytic reduction of carbon dioxide to methanol. Angew. Chem. Int. Ed. *55*, 6771–6775.

99. Feng, J., Gao, H., Feng, J., Liu, L., Zeng, S., Dong, H., Bai, Y., Liu, L., and Zhang, X. (2020). Morphology modulation-engineered flowerlike In_2S_3 via ionothermal method for efficient CO_2 electroreduction. ChemCatChem *12*, 926–931.

100. Yang, D., Zhu, Q., Sun, X., Chen, C., Guo, W., Yang, G., and Han, B. (2020). Electrosynthesis of a defective indium selenide with 3D structure on a substrate for tunable CO_2 electroreduction to syngas. Angew. Chem. Int. Ed. *132*, 2374–2379.

101. Asadi, M., Kim, K., Liu, C., Addepalli, A.V., Abbasi, P., Yasaei, P., Phillips, P., Behranginia, A., Cerrato, J.M., and Haasch, R. (2016). Nanostructured transition metal dichalcogenide electrocatalysts for CO_2 reduction in ionic liquid. Science *353*, 467–470.

102. Yang, D., Zhu, Q., Chen, C., Liu, H., Liu, Z., Zhao, Z., Zhang, X., Liu, S., and Han, B. (2019). Selective electroreduction of carbon dioxide to methanol on copper selenide nanocatalysts. Nat. Commun. *10*, 677.

103. Liu, X., Yang, H., He, J., Liu, H., Song, L., Li, L., and Luo, J. (2018). Highly active, durable ultrathin $MoTe_2$ layers for the electroreduction of CO_2 to CH_4. Small *14*, 1704049.

104. Kumar, B., Asadi, M., Pisasale, D., Sinha-Ray, S., Rosen, B.A., Haasch, R., Abiade, J., Yarin, A.L., and Salehi-Khojin, A. (2013). Renewable and metal-free

carbon nanofibre catalysts for carbon dioxide reduction. Nat. Commun. *4*, 2819.

105. Sun, X., Kang, X., Zhu, Q., Ma, J., Yang, G., Liu, Z., and Han, B. (2016). Very highly efficient reduction of CO_2 to CH_4 using metal-free N-doped carbon electrodes. Chem. Sci. *7*, 2883–2887.

106. Deng, G., Li, X., Liu, S., Zhang, Z., Lu, Z., and Guo, Y. (2016). Successive adsorption of cations and anions of water-1-butyl-3-methylimidazolium methylsulfate binary mixtures at the air-liquid interface studied by sum frequency generation vibrational spectroscopy and surface tension measurements. J. Phys. Chem. C *120*, 12032–12041.

107. Tanner, E.E.L., Batchelor-McAuley, C., and Compton, R.G. (2016). Carbon dioxide reduction in room-temperature ionic liquids: the effect of the choice of electrode material, cation, and anion. J. Phys. Chem. C *120*, 26442–26447.

108. Lim, H.K., Kwon, Y., Kim, H.S., Jeon, J., Kim, Y.H., Lim, J.A., Kim, B.S., Choi, J., and Kim, H. (2018). Insight into the microenvironments of the metal-ionic liquid interface during electrochemical CO_2 reduction. ACS Catal. *8*, 2420–2427.

109. Wang, Y., Hatakeyama, M., Ogata, K., Wakabayashi, M., Jin, F., and Nakamura, S. (2015). Activation of CO_2 by ionic liquid Emim-BF_4 in the electrochemical system: a theoretical study. Phys. Chem. Chem. Phys. *17*, 23521–23531.

110. Li, J., Wang, Z., McCallum, C., Xu, Y., Li, F., Wang, Y., Gabardo, C.M., Dinh, C.T., Zhuang, T., Wang, L., et al. (2019). Constraining CO coverage on copper promotes high-efficiency ethylene electroproduction. Nat. Catal. *2*, 1124–1131.